

1 NeuroSC: Exploring 2 Neurodevelopment via 3 Spatiotemporal Collation of 4 Anatomical Networks

5 Noelle L. Koonce^{1‡}, Sarah E. Emerson^{1‡}, Dhananjay Bhaskar², Manik Kuchroo²,
6 Mark W. Moyle^{1,11}, Pura Arroyo-Morales¹, Nabor Vázquez Martínez¹, Jamie I.
7 Emerson³, Smita Krishnaswamy^{2,4,5,6}, William Mohler^{7*}, Daniel
8 Colón-Ramos^{1,8,9,10*}

*For correspondence:

daniel.colon-ramos@yale.edu (DCR);
wmohler@neuron.uhc.edu (WM)

†These authors contributed
equally to this work

9 ¹Department of Neuroscience and Department of Cell Biology, Wu Tsai Institute, Yale
10 University, New Haven, CT, USA; ²Department of Genetics, Yale School of Medicine, New
11 Haven, CT, USA; ³Bilte Co. Ventura, CA, USA; ⁴Department of Computer Science, Yale
12 University, New Haven, CT, USA; ⁵Program for Computational Biology and
13 Bioinformatics, Yale University, New Haven, CT, USA; ⁶Program for Applied Mathematics,
14 Yale University, New Haven, CT, USA; ⁷Department of Genetics and Genome Sciences
15 and Center for Cell Analysis and Modeling, University of Connecticut Health Center,
16 Farmington, CT, USA; ⁸MBL Fellow, Marine Biological Laboratory, Woods Hole, MA, USA;
17 ⁹Wu Tsai Institute, Yale University, New Haven, CT, USA; ¹⁰Instituto de Neurobiología,
18 Recinto de Ciencias Médicas, Universidad de Puerto Rico, San Juan, Puerto Rico;
19 ¹¹Department of Biology, Brigham Young University-Idaho, Rexburg, ID, USA

20
Abstract Volume electron microscopy (vEM) datasets such as those generated for connectome
21 studies allow nanoscale quantifications and comparisons of the cell biological features
22 underpinning circuit architectures. Quantifying cell biological relationships in the connectome
23 yields rich, multidimensional datasets that benefit from data science approaches, including
24 dimensionality reduction and integrated graphical representations of neuronal relationships. We
25 developed NeuroSC (*also known as NeuroSCAN*) an open source online platform that bridges
26 sophisticated graph analytics from data science approaches with the underlying cell biological
27 features in the connectome. We analyze a series of published *C. elegans* brain neuropils and
28 demonstrate how these integrated representations of neuronal relationships facilitate
29 comparisons across connectomes, catalyzing new insights into the structure-function
30 relationships of the circuits and their changes during development. NeuroSC is designed for
31 intuitive examination and comparisons across connectomes, enabling synthesis of knowledge
32 from high-level abstractions of neuronal relationships derived from data science techniques to
33 the detailed identification of the cell biological features underpinning these abstractions.

36 **Introduction**

37 Neural circuit structure supports function. The underlying image data that yields anatomical con-
38 nectomes (or wiring diagrams) are typically obtained using volume electron microscopy (vEM) tech-

39 niques (*Collinson et al., 2023*). Since the first complete connectome was published for *C. elegans*
40 (*White et al., 1986*), these last decades have seen an increase in the generation of vEM datasets,
41 as reviewed in (*Kaiser, 2023*) and others. The expansion in available anatomical connectomes has
42 resulted from recent advancements in: 1) data generation (via automation of EM data acquisition
43 (*Xu et al., 2017; Eberle and Zeidler, 2018; Zheng et al., 2018; Phelps et al., 2021*); and 2) alignment,
44 segmentation and reconstruction (including recent implementation of AI-driven methods) as re-
45 viewed in (*Galili et al., 2022; Choi et al., 2024*) and others. As these developing methodologies
46 continue to improve, they will continue to facilitate the generation of additional connectomes of
47 whole brains and organisms.

48 The increasing availability of vEM datasets, including the first series of developmental connec-
49 tomes published for *C. elegans* (*Witvliet et al., 2021*) has highlighted the need for new tools to
50 enable intuitive examination and comparisons across connectomes to promote novel discoveries
51 (*Kasthuri et al., 2015; Lichtman et al., 2014; Barabási et al., 2023; Xu et al., 2021*). It has also un-
52 derscored the fact that vEM datasets contain a wealth of untapped information that has yet to be
53 fully examined, represented and integrated for more comprehensive analyses (*Perez et al., 2014;*
54 *Brittin et al., 2021*). For example, vEM datasets enable nanoscale explorations of the underlying
55 cell biological features that govern the properties of neural circuit architectures (*Rivlin et al., 2024;*
56 *Brittin et al., 2021; Moyle et al., 2021; Witvliet et al., 2021; Heinrich et al., 2021; Cuentas-Condori*
57 *et al., 2019*). Yet most of these cell biological features (cell morphologies, contact profiles, organelle
58 positions and shapes, etc) are not currently represented in most anatomical connectomes. Quan-
59 tification of cell biological data result in high-dimensional datasets that require new approaches for
60 their analyses and representations. The advances in vEM data generation and the resulting need
61 for new methodologies in data science and integrated representations of neuronal relationships
62 (e.g. from neuronal positions to neuropil structures) is akin to how advances in genetic sequenc-
63 ing required new methodologies in bioinformatics and new, integrated representations of genomic
64 data (e.g. from gene sequence to gene structure) (*Swanson and Lichtman, 2016*). Addressing this
65 gap holds the promise of integrating new knowledge from the fields of cell biology, neurodevel-
66 opment, physiology and systems neuroscience towards explaining how nervous system structure
67 underpins its function.

68 Most representations of anatomical connectomes have focused on defining neuronal relation-
69 ships at the level of the chemical synapse (NemaNode; WormWiring; EleganSign; FlyWire) (*Witvliet*
70 *et al., 2021; Cook et al., 2019; Fenyves et al., 2020; Dorkenwald et al., 2023*). While the existence
71 of chemical synapses between neuron pairs is an important feature of neuronal communication,
72 these representations do not capture other neuroanatomical features that also underlie neuron
73 structure and function, including contact sites from adjacent (or nearby) neurons. Recent work in *C.*
74 *elegans* examined neuronal relationships by quantifying neuron-neuron contact sites to build con-
75 tact profiles, or contactomes (*Brittin et al., 2021*). Examination of the contactome with data science
76 approaches uncovered structural principles that were not evident from interrogating the synaptic
77 connectome alone (*Moyle et al., 2021; Brittin et al., 2021*). These included the existence of higher-
78 order structural motifs and the stratification of neurons (*Moyle et al., 2021*), whose hierarchical
79 assembly during development is guided by centrally located pioneer neurons (*Rapti et al., 2017*).
80 Moreover, integrating neuronal adjacencies (contactome) with synaptic profiles (connectome) al-
81 lowed for a deeper understanding of the functional segregation of neurons within the stratified
82 neuropil structures (*Brittin et al., 2021; Moyle et al., 2021*). Key to achieving this were data sci-
83 ence approaches such as Diffusion Condensation (DC) and C-PHATE (*Brugnone et al., 2019; Moon*
84 *et al., 2019*), which resulted in reduced dimensionality of the neuronal relationships, revealing ar-
85 chitectural motifs across various scales of granularity, from individual neurons within circuits, to
86 individual circuits within the neuropil. These techniques produced graphs that enabled exploration
87 of these computationally identified groups (*Moyle et al., 2021*). DC/C-PHATE graphs are powerful
88 tools, but they have yet to be integrated to connectomics datasets as to enable explorations of the
89 underlying cell biological features. This limits their effectiveness for hypothesis generation and

90 comparative analyses across connectomes.

91 To address this, we generated NeuroSC, a tool for exploring neuroarchitectures across vEM
92 datasets via novel representations of the connectome, contactome, and anatomical networks. Neu-
93 roSC is an online, open-source platform that facilitates comparisons of neuronal features and rela-
94 tionships across vEM data to catalyze new insights of the relationships that underpin architectural
95 and functional motifs of the nerve ring neuropil. NeuroSC builds on recent publications in whole-
96 brain EM datasets, integrating the latest set of developmental connectomes (*Witvliet et al., 2021*)
97 and employing data science tools (*Brugnone et al., 2019; Moon et al., 2019*) to examine neuronal
98 relationships based on contact profiles. NeuroSC was purposefully developed with a different and
99 complementary goal to existing tools that offer web-based visualization and access to large-scale
100 EM datasets, such as NeuroGlancer and Webknossos (*Maitin-Shepard et al. (2021); Boergens et al.*
101 *(2017)*). The explicit goal of NeuroSC is to provide a platform optimized for examining *neuronal*
102 *relationships* across connectomic datasets. To achieve this NeuroSC builds on the segmentations
103 emerging from programs like NeuroGlancer and Webknossos, but with tools tailored to explore re-
104 lationships such as contact profiles in the context of neuronal morphologies and synaptic positions,
105 and across datasets that represent different animals or different developmental stages. Designed
106 as an open-source and modular platform, NeuroSC is intended to integrate with these existing
107 tools and datasets, supporting a synergistic approach to navigating, analyzing, and deriving mean-
108 ing from complex connectomic resources.

109 We demonstrate how these integrated representations of neuronal relationships facilitate com-
110 parisons across these connectomes, catalyzing new insights on their structure-function and changes
111 during development. NeuroSC achieves this by addressing three challenges in current neuronal
112 representations: 1) accessibility of specific neuronal cell biological features (i. e. synapses and
113 contacts), 2) integration of features for examining neuronal relationships across anatomical scales,
114 and 3) spatiotemporal comparisons of these features across developmental datasets. These chal-
115 lences were addressed by 1) creating representations of contact sites and establishing the ability to
116 visualize subsets of synaptic sites; 2) enabling synchronous visualization of neuron morphologies,
117 contacts and synapses and integrating these cell biological features with algorithmically-generated
118 graphical representations of neuronal relationships; and 3) enabling simultaneous exploration of
119 these relational representations across developmental connectomes. NeuroSC was designed as a
120 suite of tools that facilitates future incorporation of additional datasets and representations with
121 the goal of enabling integrated data exploration beyond the available *C. elegans* connectomes. The
122 NeuroSC-based approaches used here for *C. elegans* could be applicable to other systems as new
123 EM-based datasets and reconstructions become available.

124 **Results (Comparing contactome-based relationships using C-PHATE.)**

125 The adult hermaphrodite *C. elegans* nerve ring is a neuropil of 181 neurons of known identities, mor-
126 phologies, contact profiles, and synaptic partners (*White et al., 1986*). Even for this relatively small
127 neuropil, representations of a single feature type, such as neuronal contact profiles, constitute over
128 100,000 data points of multidimensional information: cell identity, region of contact, presence of
129 synapses, etc. Analysis of this multidimensional information requires approaches that can both
130 capture higher-order patterns of organization while enabling researchers to access the underlying
131 cell biological features resulting in these relationships. We implemented Diffusion Condensation
132 (DC), a clustering algorithm that iteratively groups neurons based on the quantitative similarities
133 of their 'contact' or 'adjacency' profiles (*Brugnone et al., 2019; Moyle et al., 2021*). Briefly, DC makes
134 use of pair-wise quantifications of adjacent neuron contacts to, in a graph, move neurons with sim-
135 ilar adjacency profiles closer together by applying a diffusion filter in a multidimensional manifold.
136 At each iteration, the diffusion filter smooths the data across the manifold, such that local vari-
137 ability (or noise) in the adjacency profiles is reduced, highlighting broader, higher order pattern
138 similarities across neurons. As iterations proceed, individual neurons (and eventually groups of
139 neurons) are clustered together based on how close their contact profiles are to one another in

140 the manifold (**Brugnone et al., 2019**). In this way, DC uncovers hierarchical neuronal relationships
141 in the contactome (**Moyle et al., 2021**).

142 To ensure accurate comparisons of DC across available EM datasets (**Witvliet et al., 2021; White**
143 **et al., 1986**), we empirically determined minimum-distance adjacency thresholds (measured in pix-
144 els; Supplementary Table 1) to construct adjacency profiles. Each neuron's adjacency profile is a
145 quantitative measure that captures the extent of contact with neighboring neurons within its spa-
146 tial vicinity. By individually setting distance thresholds for each dataset, we ensured that the degree
147 of adjacency—defined by both the presence and extent of contact—could be accurately compared
148 across datasets generated at different times and using diverse methodologies (see also Methods
149 and Materials), schematized in Figure 1A-C). We applied an established adjacency algorithm to
150 quantify the extent of contact between neuron pairs by measuring the number of shared pixels
151 within the defined distance threshold for adjacency (**Brittin et al., 2021**). Pixel counts were summed
152 for each neuron across EM slices within the defined nerve ring region (see Methods), resulting in
153 an adjacency matrix representing pairwise shared pixel counts for each of the seven selected *C.*
154 *elegans* contactome datasets (L1, 0 hours post hatch (hph); L1, 5hph; L2, 16hph; L3, 27hph; L4,
155 36hph; Adult 48hph (Figure 1C; See also Methods and Materials). These adjacency matrices were
156 fed into DC to reveal iterative clusters of neurons with similar adjacency profiles. To visualize and
157 compare the results from DC, we used a graphical representation of the algorithm output called
158 C-PHATE (**Moon et al., 2019; Moyle et al., 2021**), a 3-D visualization tool that builds a hierarchical,
159 visual representation of the DC agglomeration procedure (Figure 1D-E). In C-PHATE visualizations,
160 the DC output is mapped in 3-D space with spheres. Initially, all individual neurons in the neuropil
161 dataset are at the periphery of the C-PHATE graph (left hand side in schematic in Figure 1D, edges
162 of graph in Figure 1E). Neurons are iteratively condensed together based on the similarity of their
163 adjacency profiles (schematized in Figure 1D). In the last iteration of DC, there is a single point at
164 the center of the C-PHATE graph which represents the entire neuropil (Figure 1E, red dot). C-PHATE
165 representations enable visualization and comparisons of contactomes across datasets, and explo-
166 rations of neuronal relationship trajectories, from individual neuron interactions to circuit-circuit
167 bundling (Figure 1F and Figure 2).

168 By Larval stage 1 (L1) 90% of neurons in the neuropil (161 neurons out of the 181 neurons)
169 have grown into the nerve ring and adopted characteristic morphologies and positions. Although
170 the organism grows approximately 5 fold from L1 to the adult, contacts in the nerve ring are also
171 largely established by L1 and preserved during postembryonic growth (**Witvliet et al., 2021**). In
172 agreement with this, when we used DC and C-PHATE to examine contactomes from these datasets
173 we consistently identified four main super clusters—Stratum 1, Stratum 2, Stratum 3, and Stratum
174 4, using the clusters found at the highest modularity score (the iteration at which the algorithm
175 has the highest clustering confidence) (**Newman, 2006**) (Figure 2B-F). DC outputs for each strata
176 across animals can also be inspected using Sankey diagrams (Supplemental Tables 3-6). These
177 diagrams detail the neuron members at each iteration of DC, allowing the user to derive quan-
178 titative comparisons of clustering events. The alignment of the neuronal morphologies of strata
179 members reveals a persistent layered organization to the nerve ring neuropil (Figure 2 G-K), and
180 the functional identities of the neurons in each stratum suggests that there is spatial segregation
181 of sensory information and motor outputs (**Moyle et al., 2021**), Supplementary Tables 3, 4, 5, 6).
182 Our findings are consistent with previous studies on the Larval Stage 4 (L4) and adult contactomes
183 (**Moyle et al., 2021**), and support that neurons establish core relationships during embryogene-
184 sis and maintain them during postembryonic growth, consistent with previous studies (**Witvliet**
185 **et al., 2021**). Our findings also demonstrate the utility of DC and C-PHATE analyses in extracting,
186 visualizing and comparing the structure of the neuropil architecture across contactomes.

187 Because DC and C-PHATE allow for the examination of relationships at varying levels of gran-
188 ularity, these diagrams also facilitate the interrogation of the architectural motifs that underlie
189 distinct neural strata. A more detailed examination of clusters reveals that while the overall strata
190 are preserved, the underlying neuronal configurations undergo changes during postembryonic

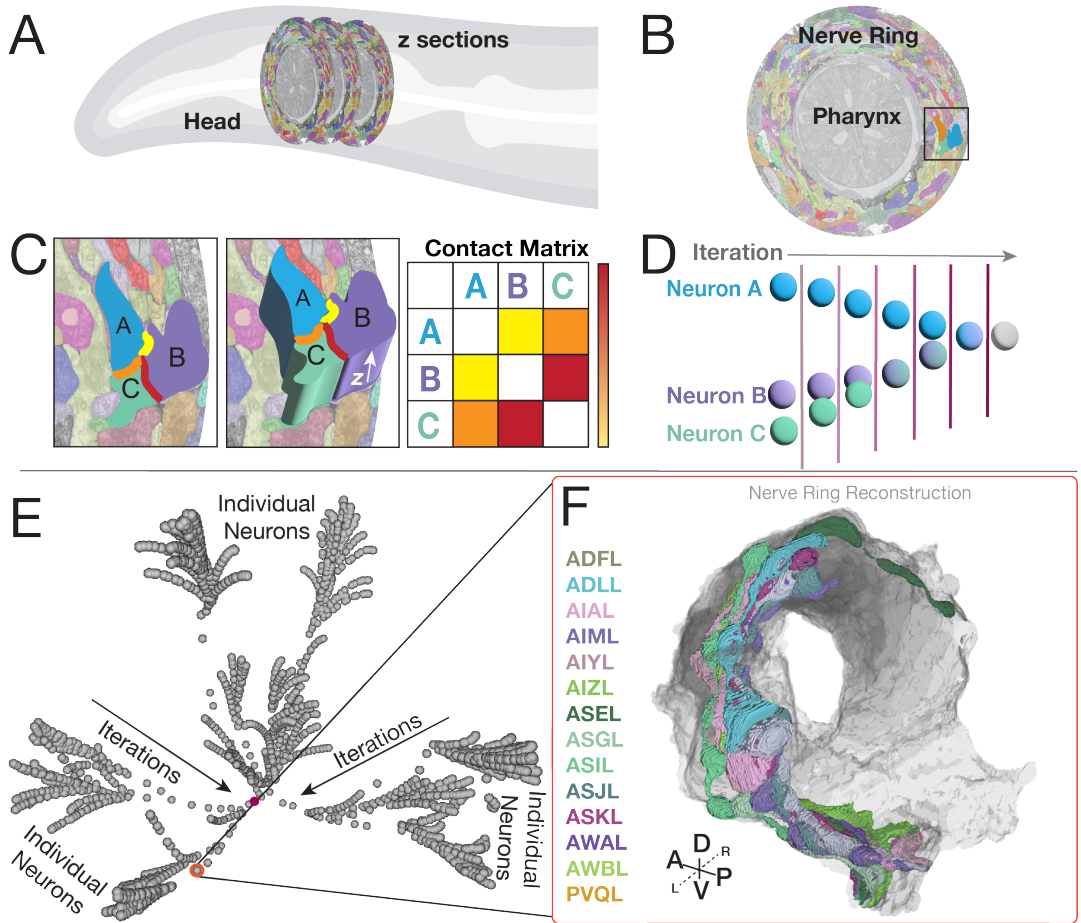


Figure 1. DC/C-PHATE representations of contactome-based relationships. DC/C-PHATE graphs enable representations of neuronal contact relationships. To build DC/C-PHATE graphs we (**A**) analyzed serial section EM datasets of the *C. elegans* nerve ring neuropil (located in the head of the animal). (**B**) Single cross section of the nerve ring (surrounding the pharynx), with segmented neurites pseudo-colored. Dark box corresponds to the zoomed-in image in (**C**). The cross section is from the JSH dataset digitally segmented ([Brittin et al., 2021](#)). (**C**) Zoom-in cross section with three arbitrary neurons (called A, B, C) highlighted by overlaying opaque cartoon (2-D, left image) and 3-D shapes (middle image) to represent the segmentation process in the z-axis (arrow) and the neuronal contact sites (highlighted Yellow, orange and Red). Contacts are quantified for all neuron pairs across the contactome (See Methods), to generate a Contact Matrix (represented here as a table, schematized for the three arbitrary neurons selected and in which specific contact quantities are represented by a color scale and not numerical values). Yellow represents little contact, and red represents a large degree of contact. Here, as an example you can see that neuron B and C have the largest degree of contact. In an actual contact matrix, this would be a large number of shared pixels. (**D**) Schematic of how the Diffusion Condensation algorithm (visualized with C-PHATE) works. DC/C-PHATE makes use of the contact matrix to group neurons based on similar adjacency profiles ([Brugnone et al. 2019; 2019; Moyle et al. 2021](#)), schematized here for the three neurons in (**C**). (**E**) Screenshot of the 3-D C-PHATE graph from a Larval stage 1 (L1; 0 hours post hatching) contactome, with individual neurons represented as spheres at the periphery. Neurons were iteratively clustered towards the center, with the final iteration containing the nerve ring represented as a sphere in the center of the graph (Highlighted in maroon). (**F**) Integration in NeuroSC of the DC/C-PHATE and EM-derived 3-D neuron morphology representations allow users to point to each sphere in the graph and determine cellular or cluster identities for each iteration. Shown here and circled in Red, an arbitrarily selected cluster (in **E**), with the identities of the neurons belonging to that cluster (four letter codes in the column to the left of **F**) and the corresponding neuronal morphologies (right) of this group of neurons in the EM-reconstructed nerve ring (with individual neurons pseudo-colored according to their names to the left). Compass: Anterior (A), Posterior (P), Dorsal (D), Ventral (V), Left (L), Right (R).

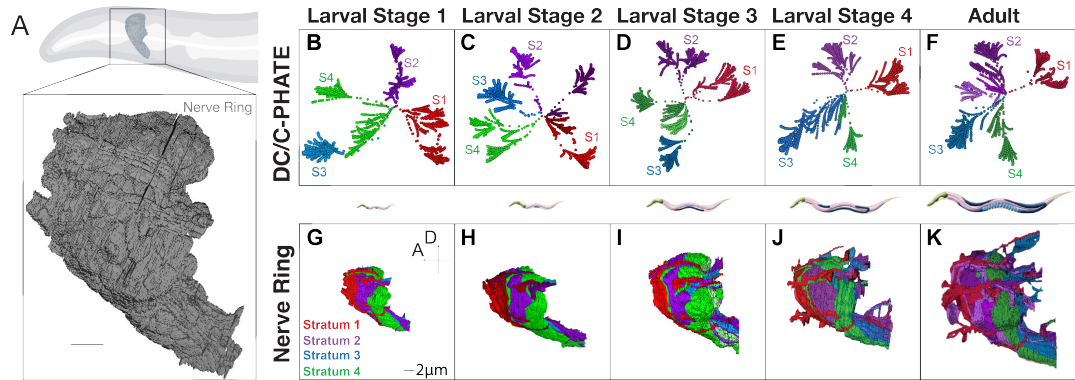


Figure 2. Implementation of DC/C-PHATE to developmental contactomes reveal a conserved layered organization maintained during post-embryonic growth. (A) Cartoon of the *C. elegans* head and nerve ring (outlined with black box). Below, nerve ring reconstruction from EM data of an L1 animal (5 hours post hatching), with all neurons in gray. Scale bar 2 μ m. (B-F) DC/C-PHATE plots generated for available contactomes across *C. elegans* larval development, colored by stratum identity as described (Moyle et al., 2021). Individual neurons are located at the edges of the graph and condense centrally. The four super-clusters identified and all iterations before are colored accordingly. The identity of the individual neurons belonging to each stratum, and at each larval stage, were largely preserved, and are provided in Supplementary Tables 3-6. Some datasets contain 5 or 6 super-clusters (colored hues of the stratum that they most closely identify with). These clusters are classified as groups of neurons that are differentially categorized across the developmental connectomes. Note in B the blue cluster extends far to the left due to rotation of the 3D image. (G-K) Volumetric reconstruction of the *C. elegans* neuropil (from EM serial sections for the indicated larval stages (columns) with the neurons colored based on their strata identity. Scale bar 2 μ m; Anterior (A) left, Dorsal (D) up.

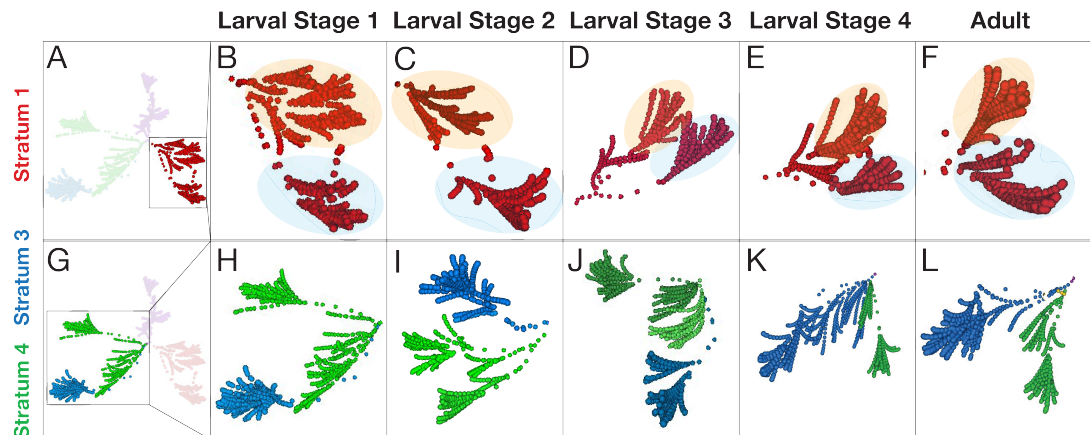


Figure 3. Examination of the architectural motifs underlying the distinct strata across development. Visualization of (A-F) Stratum 1 (Red) and (G-L) Strata 3 and 4 (Blue and Green) reveal motifs that are preserved (Stratum 1) and change (Strata 3 and 4) across developmental contactomes (L1 to Adult, left to right, as indicated by labels on top). (B-F) Cropped view of Stratum 1 at each developmental stage showing a similar shape of two 'horn-like' clusters in the C-PHATE graphs (as seen by orange and blue shaded areas). These two clusters have similar neuronal memberships, which are largely invariant across developmental contactomes (Supplementary Table 3). (H-L) Cropped view of Strata 3 and 4 at each developmental stage highlighting differences in the organization and number of neurons contained in each of the Blue and Green strata, which is particularly distinct when comparing (H) L1 and (K) L4 (Supplementary Tables 5, 6).

6).

191 growth (Figure 2 B-F, Figure 3, see: Supplementary Tables 3, 4, 5, 6). Three general features were
192 extracted from these analyses: 1) individual neurons renegotiate their positions in the context of
193 the identified C-PHATE clusters in different developmental contactomes, suggesting developmen-
194 tal changes; 2) the degree of these changes varied across the distinct strata; and 3) the degree
195 of these changes mapped onto strata containing neurons with functions known to require either
196 more or less neuronal plasticity, such as integrative behaviors versus more fixed reflexive behav-
197 iors, respectively. For example, Stratum 1, which contains most neurons contributing to shallow
198 reflex circuits, controlling aversive head movements in response to noxious stimuli, displayed the
199 fewest changes among the developmental connectomes (Figure 3 B-F; Supplementary Table 3).
200 On the other hand, *C. elegans* exhibit tractable behaviors which can adapt due to changing environ-
201 mental conditions **Flavell et al. (2020)**. Strata 3 and 4 contain most neurons belonging to circuits
202 associated with such learned behaviors, including chemo, mechano and thermo sensation. This is
203 reflected by strata 3 and 4 being the regions of the most change in neuronal relationships across
204 postembryonic development (Figure 3G-L; Supplementary Tables 5, 6).

205 To examine the changes in DC/C-PHATE during postembryonic development, we made the C-
206 PHATE plots fully interactive. This enables users to hover over and identify members of each inter-
207 mediate cluster, to highlight specific cell trajectories via pseudo-coloring, and compare specific neu-
208 ronal relationship dynamics across development within a multi-view window of distinct C-PHATE
209 plots (Figure 1 E-F, Supplementary Figure 6, Supplementary Video 1). Because C-PHATE graphs ult-
210 imately represent cells of known identities, we reasoned that interactive mapping of the C-PHATE
211 cluster objects to their component cellular identities and anatomies could yield greater insights on
212 neurodevelopmental changes by linking the algorithmic abstractions of the relationships with the
213 cell biological features and their changes across development (Figure 4).

214 To evaluate our hypothesis and assess the utility of C-PHATE for discovery, we examined spe-
215 cific regions where the distribution or 'shape' of super clusters changed across developmental con-
216 tactomes. This approach accounts for differences in contact profiles, which directly impacts the
217 overall clustering structure. Based on these criteria, we focused on a region displaying changes in
218 Strata 3 and 4 and using the interactive C-PHATE graphs (Figure 4 A-E), we determined the identities
219 of neurons that changed clustering patterns across the developmental contactomes. Specifically,
220 we focused on two interneurons, named AIML and PVQL, which we observed undergo a change
221 in their cluster assignment from Stratum 4 (at L1) to Stratum 3 (at Larval stage 4, L4; Figure 4A
222 and D). We pseudo-colored the trajectories of the AIML and PVQL neurons in C-PHATE to explore
223 the changes in their C-PHATE trajectories throughout the developmental stages (Figure 4F-I, Sup-
224 plimentary Figure 1, Supplementary Table 7). Comparison of the identities of the neurons that
225 co-cluster with AIML and PVQL suggests that the contact relationships varied across developmen-
226 tal stages (Figure 4F and G, Supplementary Figure 1), co- cluster members can also be evaluated
227 via Sankey diagrams, showing a switch in membership of AIM and PVQ from clusters of stratum 4
228 at L1- L2, pre-AVF ingrowth, to include a transitional stratum at L3, finally to stratum 3 at L4-adult
229 after AVF ingrowth, (see Supplementary Table 7).

230 **Visualizing contact profiles in individual cells.**

231 DC/C-PHATE changes should result from changes in contact profiles. To link the observed changes
232 in the C-PHATE graphs with the cell-biological changes in contact profiles, we generated a tool that
233 would simultaneously enable: 1) 3D visualization of the cell-cell contact sites onto individual neu-
234 ronal morphologies; 2) examination and comparisons of these contact profiles throughout devel-
235 opment for the available contactomes; and 3) integration with DC/C-PHATE to link C-PHATE cluster
236 objects to the 3-D morphologies of the algorithmically clustered cells. With these capabilities inte-
237 grated, we could simultaneously view the contactome from two complementary perspectives – at
238 an abstract systems level via DC/C-PHATE and at a cell biological level via 3D contact modeling – to
239 perceive the architectural themes that underlie similar network patterns.

240 To create this tool, we generated 3D models of the area of physical contact between adjacent

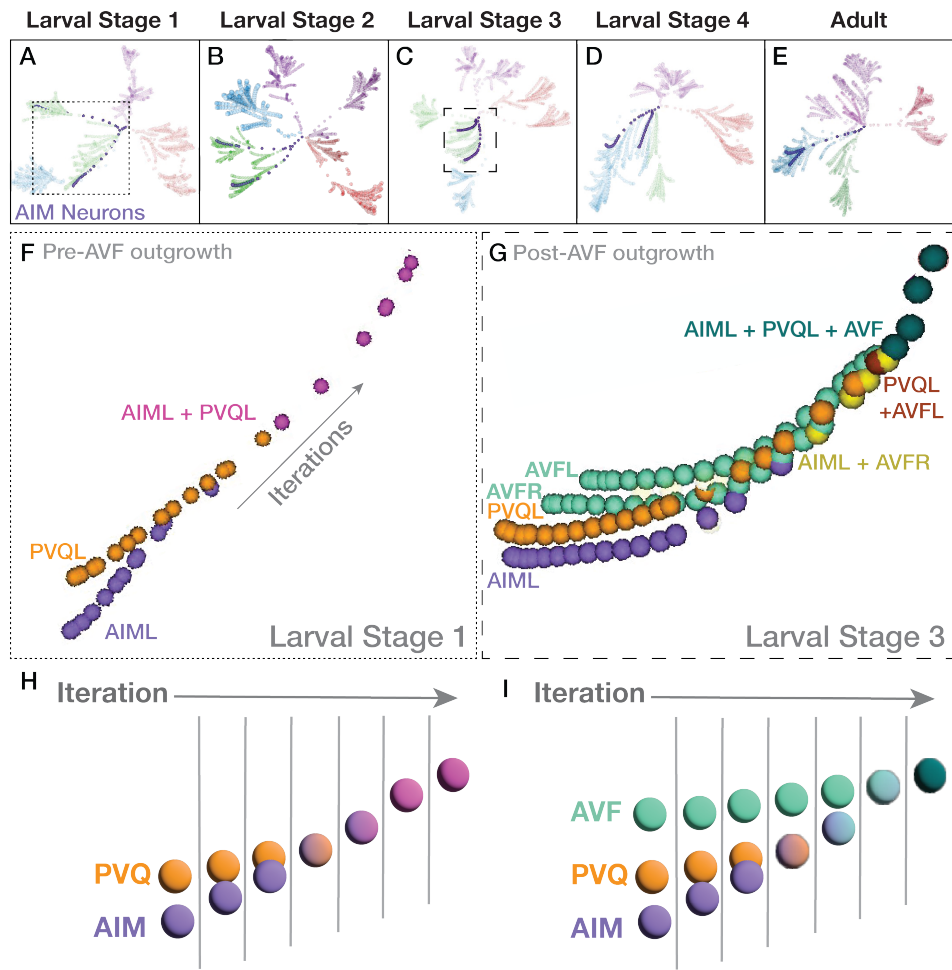


Figure 4. Case study: AIML and PVQL neurons change clustering patterns across the developmental contactomes. (A-E) C-PHATE plots across development, with the trajectories of AIM neurons (in purple) and the rest of the spheres colored by stratum identity (see Figure 2). **(F-G)** Zoom in of the AIML and PVQL trajectories corresponding to larval Stage 1 (pre-AVF ingrowth) (A, dotted box) and in (G), Larval Stage 3 with AVFL/R present (C, dashed box). Note how the relationship between AIM and PVQ neurons in the C-PHATE graph varies for each of the examined contactomes across development. (Supplementary Figure 1, Supplementary Table 7). **(H,I)** simplified schematics of F and G based on neuron class.

241 neuron pairs (Supplementary Tables 1, 2; Methods and Materials; Figure 5) (Supplementary Figure
242 2). Visualizing contacts from all adjacent neurons builds a multi-colored skeleton of the neuron
243 morphology mapped onto the boundaries of this neuron (Figure 5A and C). Because the identities
244 of the neurons are known and linked to the 3D contact models, we built text pop-ups that define
245 the contact partners for each site (Figure 5C). Furthermore, since neuron names are consistent
246 across the EM datasets, we can link and compare contact sites throughout development (Figure 5
247 D). Additionally, we can analyze the representations of contact sites in the context of DC/C-PHATE
248 clustering profiles (Figure 4F-I), 3D models of neuronal morphologies (Figure 1F), and 3D models
249 of synaptic sites for any neuron(s) across development (Figure 7).

250 We used the integrated tools of DC/C-PHATE and 3D representations of the contact profiles
251 to examine the potential cell biological changes leading to the DC/C-PHATE clustering changes ob-
252 served for the AIML neuron during development. With these tools, we observed changes in the
253 identities of the contacts made in the dorsal region of the AIML neurite (Figure 5D; Supplemen-
254 tary Figure 3). Specifically, in the L2 stage (as compared to L1), we observed a decrease in the contacts
255 from PVQL and an increase in contacts from the AVF neurons. This change persists to the adult

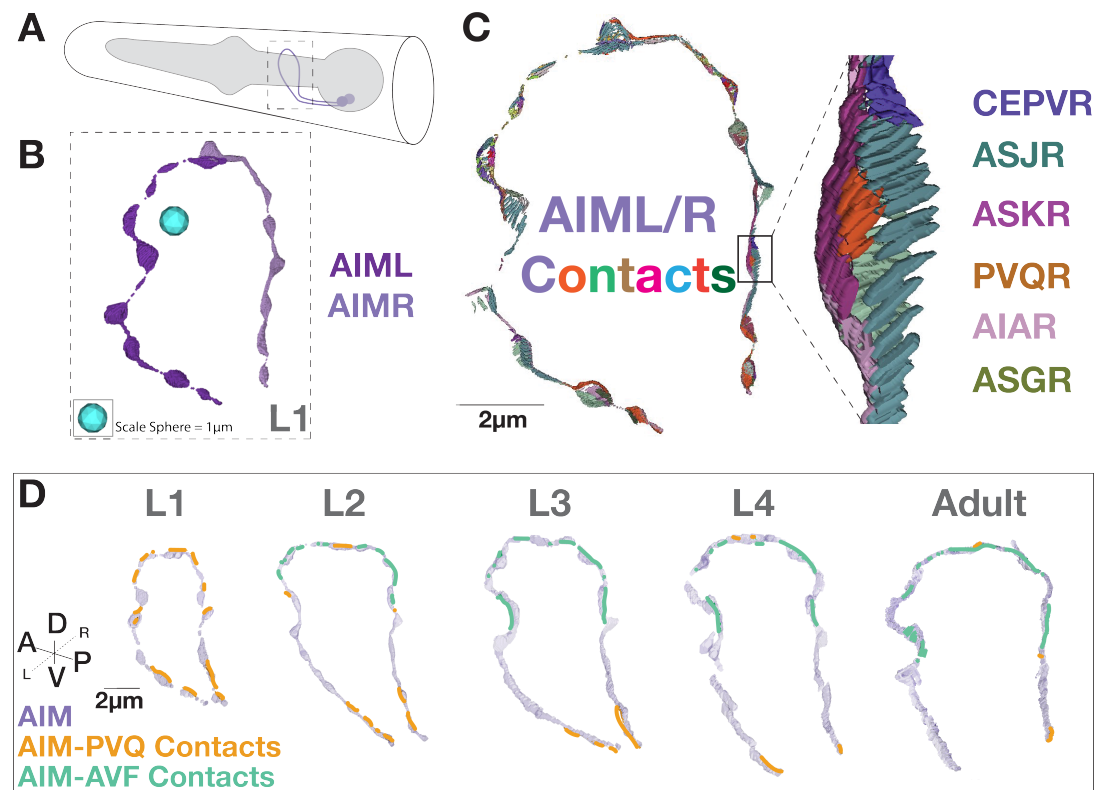


Figure 5. Case Study: Visualization of contact profiles in individual neurons. **(A)** Cartoon schematic of the head of the animal with the AIM neurons (purple) and pharynx (gray), and (dotted box) a 3-D reconstruction of the AIM neuron morphology from the L1 (0 hours post-hatching) dataset. **(B)** AIML and AIMR neurites rendered in 3D from L1. Note that we did not implement any surface smoothing methods to objects, so there might be gaps in the renderings. This was done intentionally, with the goal of producing the most accurate representation of the available data segmentation and avoid any rendering interpretations. **(C)** 3-D representation of all contacts onto the AIM neuron morphology in an L1 animal, colored based on contacting partner identity, as labeled (right) in the detailed inset (black box) region. **(D)** AIM-PVQ contacts (in orange) and AIM-AVF contacts (in green), projected onto the AIM neurons (light purple) across developmental stages and augmented for clarity in the figure (see non-augmented contacts in (Supplementary Figure 5). Scale bar 2 μ m.

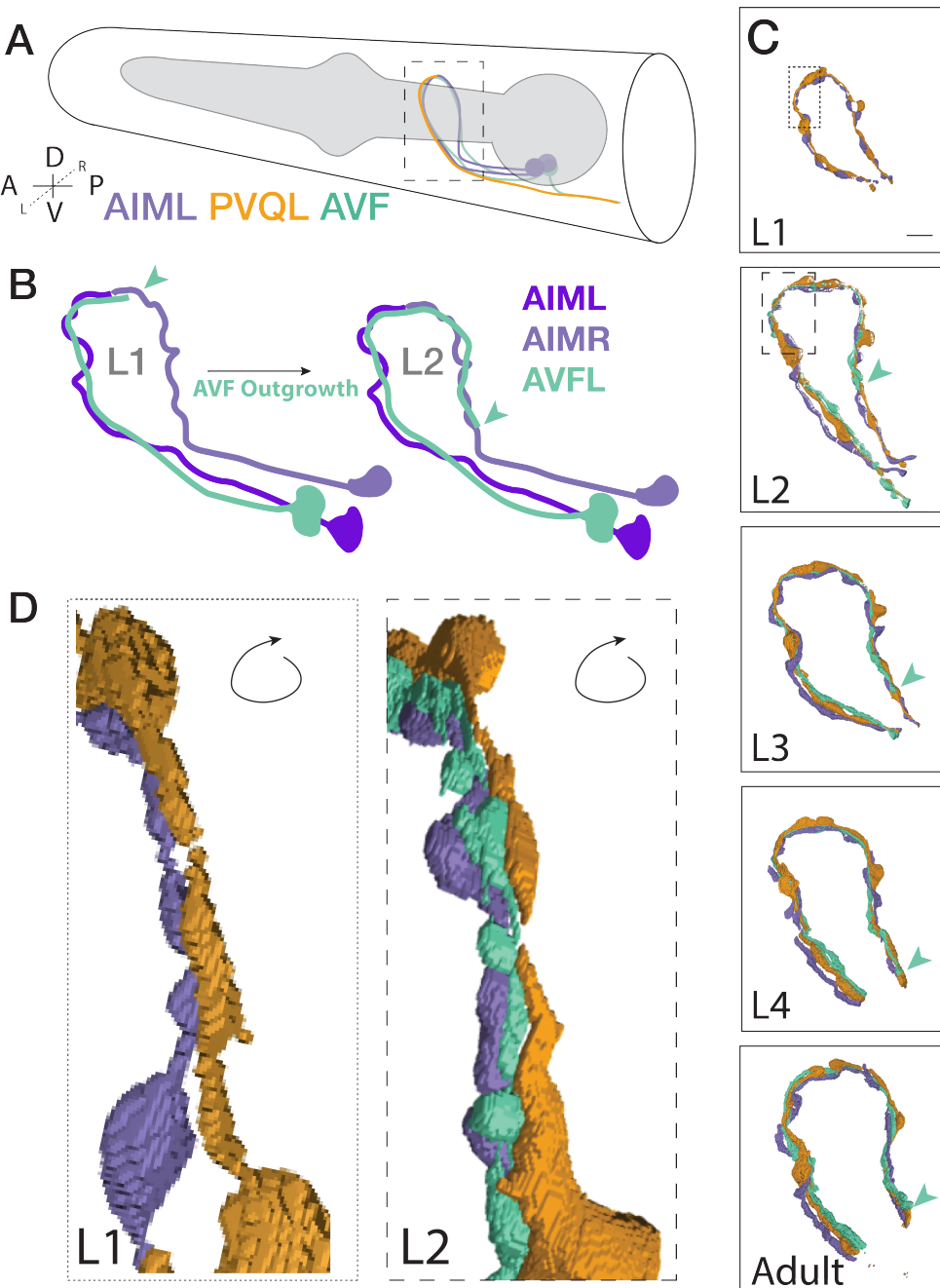


Figure 6. Case study: Segmented morphologies of AIM, PVQ and AVF across larval development. (A) Cartoon schematic of the *C. elegans* head, pharynx (gray) and examined neurons with dashed black box representing the nerve ring region. (B) Schematic representation of the outgrowth path of the AVF neurons as observed by EM (Witvliet *et al.*, 2021). Note that in development, AVFL and AVFR both grow along AIML and extend in parallel around the nerve ring. The distal end of the AVF neurite is highlighted with a green arrowhead in the schematic. (C) Neuronal morphologies of AIM (purple), PVQ (orange), AVF (green) across postembryonic development, as indicated, with green arrowhead pointing to AVF outgrowth tip. Scale bar = 2 μm . Regions for insets (L1, dotted box; L2, dashed box) correspond to (D). (D) Morphologies of these neurons (rotated to the posterior view) display the AVF neurons' positions between the AIM and PVQ neurons at the L1 and L2 stage. Indicated outgrowth between neurons continues to the Adult stage (Supplementary Video 2). Note how AVF outgrowth alters contact between PVQ and AIM (Figure 5D).

256 stage (Figure 5D; Supplementary Figure 3).

257 To then determine the possible source of these developmental changes in contacts, we visual-
258 ized 3D models of the segmented morphologies for these neurons across L1 to adulthood (Figure
259 6). We find that AIM and PVQ neurons maintain similar morphologies throughout development
260 (Figure 6C), while AVF neurons undergo substantial neurite outgrowth onto new regions of con-
261 tact between AIM and PVQ (Figure 6 B-D). These observations are consistent with lineage studies
262 which demonstrated that AVF neurons are generated from neuronal precursors (P0 and P1) at the
263 end of the L1 stage (*Sulston et al. (1983); Sun and Hobert (2023); Poole et al. (2024); Hall and Altun*
264 *(2008); Sulston and Horvitz (1977)*). By comparing the EM datasets across development, we observe
265 that the AVF neurons grow into the nerve ring during the L2 stage, and continue to grow until the
266 Adult stage (Figure 6 B-D). We also consistently observe throughout the individual datasets, that
267 the AVF neurons grow in between the AIM and PVQ neurons (Figure 6D), altering their contact
268 profiles, which likely contributes to the observed changes in the C-PHATE graphs. While the DC/C-
269 PHATE representations systematically cluster neurons based on relative similarities across contact
270 profiles, and not solely by scoring changes in specific contacts within any given pair, our findings
271 demonstrate the use of DC/C-PHATE as a discovery tool to identify cell-biological contact changes
272 during development. (Figure 4F and G; Figure 5 D; Supplementary Video 2). Consistent with this,
273 we also observe that both AVFL and AVFR grow into the nerve ring alongside AIML, later continuing
274 to grow around to reach AIMR, and that these relationships were reflected in the C-PHATE graphs
275 in terms of the clustering profiles throughout development (Figure 4G; Supplementary Figure 1).

276 We then examined if the developmental changes in contact profiles result in changes in circuitry.
277 We examined this by layering on synaptic information. Despite dwindling AIM-PVQ contacts, AIM
278 and PVQ neurons maintained their synaptic relationship throughout development, with synaptic
279 sites observed primarily at the base of AIM neurons, a region of persistent contact with PVQ (Figure
280 7A-B). We observed that increases in contacts between AIM and AVF neurons resulted in additional
281 en passant synapses at the new points of contact, beginning at the L2 stage and continuing to
282 adulthood (Figure 7A-B). We also observed that AVF forms synapses with the adjacent PVQ neurons
283 (Figure 7; Supplementary Figure 4).

284 In summary, by integrating, representing and comparing datasets using the new C-PHATE tools
285 and contact profiles in NeuroSC, we identified developmental changes in the relationships of AIM,
286 AVF and PVQ. This case-study highlights the utility of combining cell biological representations (such
287 as morphologies, contacts and synapses) with coarse-grained systems-level representations (like
288 DC/C-PHATE) of vEM datasets to uncover developmental changes which could be further explored
289 experimentally. Therefore, NeuroSC serves as a powerful platform for generating hypotheses for
290 empirical testing, which can lead to insights into the dynamics of circuit development.

291 **NeuroSC: Facilitating multi-layered interrogation of neuronal relationships in the** 292 ***C. elegans* nerve ring throughout larval development**

293 NeuroSC is built as a web-based client-server system designed to enable the sharing of anatomical
294 connectomics data with an emphasis on facilitating the analyses of neuropil relationships across
295 hierarchies and scales. To achieve this, we integrated tools of neuroanatomical investigation from
296 the available *C. elegans* nerve ring connectomes and contactomes with a collection of 3-D mod-
297 eled elements (morphologies, contacts and synapses and C-PHATE) representing different aspects
298 of neuronal architecture and relationships (Figure 8). NeuroSC differs from other available web-
299 based tools in this area with the integration of C-PHATE graphs that enable exploration of hierar-
300 chical organizations of stratified fascicles, the availability of new tools to examine the contactome,
301 and the integration of these data with existing connectome and morphological datasets across
302 developmental stages.

303 NeuroSC has eight key user-driven features: (1) C-PHATE, with the ability to highlight clusters
304 containing neurons of interest (Supplementary Figure 6, Supplementary Video 1), (2) interactive re-
305 constructions of neuronal morphologies (Supplementary Figure 10, Supplementary Video 3), with

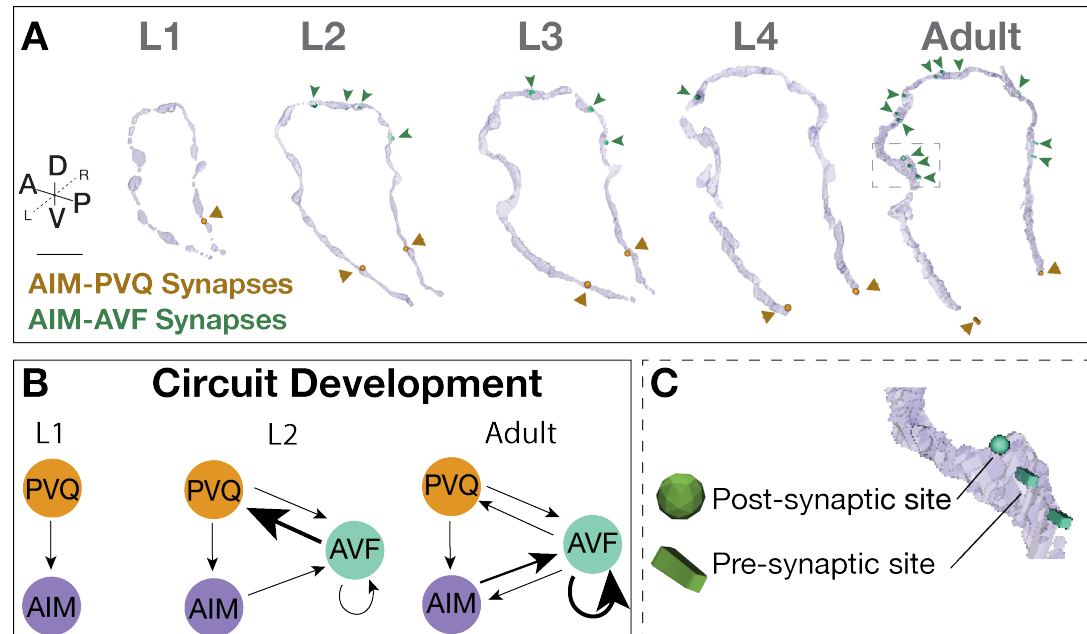


Figure 7. Case study: AIM-PVQ and AIM-AVF synaptic positions across development. **(A)** AIM-PVQ synaptic sites (dark orange arrowheads) and AIM-AVF synaptic sites (dark green arrowheads) in the segmented AIM neurons and reconstructed across postembryonic development from original connectomics data. Scale bar = 2 μ m. **(B)** Schematic of the AIM, PVQ and AVF circuitry across development based on synaptic connectivity and focusing on the stage before AVF outgrowth (L1), during AVF outgrowth (L2) and Adult; arrow direction indicates pre to post synaptic connection, and arrow thickness indicates relative number of synaptic sites (finest, <5 synapses; medium, 5-10 synapses; thickest, 11-30 synapses). **(C)** Zoom in of synaptic sites (green) in the Adult connectome and embedded into the AIM neuron morphology (light purple). In NeuroSC, presynaptic sites are displayed as blocks and postsynaptic sites as spheres, and a scaling factor is applied to the 3-D models (Materials and Methods).

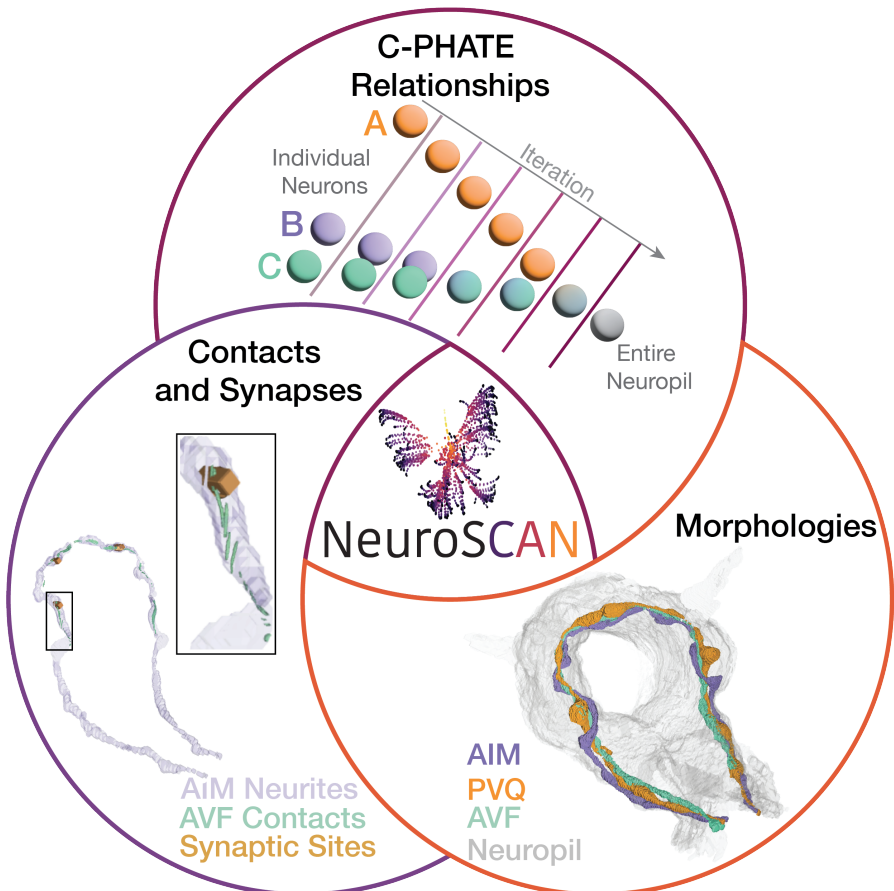


Figure 8. NeuroSC is a tool that enables integrated comparisons of neuronal relationships across development. With NeuroSC, users have integrated access to: C-PHATE plots, 3-D morphological renderings, neuronal contact sites and synaptic representations. Through stage-specific C-PHATE renderings, users can explore neuronal relationships from high dimensional contactome data. **(Top)** On C-PHATE plots, schematized here, each sphere represents an individual neuron, or a group of neurons clustered together during algorithm iterations. **(Right)** 3D renderings of select neurons can be visualized in the context of the entire nerve ring or other circuits (gray). **(Left)** AIM contact sites at L1 and the same region showing synapses. Inset shows zoomed in of contacts and synapses - presynaptic sites (blocks) and postsynaptic sites (spheres). Data depicted here are from the L1 stage (0 hours post hatching).

306 click-based display of cell statistics, including total volume and surface area within the defined
307 neuropil region (see Methods), (3) reconstructions of neuronal morphologies of C-PHATE cluster
308 members with a right-click on C-PHATE clusters (Supplementary Video 1), (4) 3-D renderings of neu-
309 ronal contacts to visualize the spatial distribution of contact profiles, with click-based displays of
310 quantitative statistics, including total contact area, rank among all contacts of the primary neuron,
311 and surface area percentages relative to both the neuron and the nerve ring (Supplementary Fig-
312 ure 5, Supplementary Video 4), (5) 3-D representations of synaptic sites with the option to visualize
313 subsets of those sites, and a click-based display showing the number of synapses of the selected
314 identity within the primary neuron, including any polyadic synapse combinations involving the pri-
315 mary neurons (Supplementary Figure 7, Supplementary Video 4) (6) the ability to perform side-by-
316 side comparisons across development by cloning a rendered scene across time into a new window
317 at the click of a button using the in viewer developmental stage slider (Supplementary Figure 11,
318 Supplementary Video 3), (7) the option to pseudo color each object to highlight points of interest
319 (Supplementary Figure 11, Supplementary Video 3) and (8) each item is an individual object with
320 the ability to be further customized by the user (Supplementary Figures 11, 12).

321 **NeuroSC: practical considerations**

322 We offer seven practical considerations for users. First, NeuroSC is available on mobile platforms
323 as a quick and convenient way to look up neuron morphologies and relationships. Second, since
324 contact sites offer the ability to explore the surrounding neurons and the position(s) of contact
325 between adjacent neurons, NeuroSC is designed to enable studies of adjacent neurons (e.g. phe-
326 notypes that result in site-specific ectopic synapses; neuron morphology changes that may affect
327 specific surrounding neurons; developmental events requiring communication between neurons,
328 etc.). Third, C-PHATE can be used to identify neurons with similar contact profiles. Because contact
329 profiles are associated with circuit identities (*Moyle et al., 2021*), exploration of neuronal rela-
330 tionships via C-PHATE can be used to identify new relationships between specific neurons and circuits.
331 Fourth, visualization of subsets of synaptic and contact sites allows direct comparisons to light mi-
332 croscopy approaches such as cell-specific labeling of synapses or GFP-Reconstitution across synap-
333 tic partners (Feinberg et al. 2008). Fifth, because the color and transparency of each 3-D model
334 can be customized, users can further integrate NeuroSC outputs of additional atlases (for gene
335 expression, neurotransmitter and receptor expression, functional connectivity, etc. (*Packer et al.,*
336 *2019; Taylor et al., 2021; Wang et al., 2023; Fenyves et al., 2020; Randi et al., 2023; Maitin-Shepard*
337 *et al., 2021*) and directly use the NeuroSC outputs to create figures and comparisons (as done for
338 this paper). Sixth, although synaptic sites with BWM (body wall muscles) are included in NeuroSC,
339 the current data model limits the ability to search for these non-neuronal cells. Users can search
340 for neurons with synapses to BWM to find this datatype. Seventh, to enable direct comparisons
341 between our data representations and the primary EM data, the original annotations have been
342 preserved and can be accessed by users via the sister app, CytoSHOW (CytoSHOW.org). As the data
343 continues to be curated, the modular design of NeuroSC and its companionship with CytoSHOW
344 enables integration of future annotations.

345 **Discussion**

346 NeuroSC is an integrative tool for analyzing detailed, web-based representations of neuronal con-
347 nectomes and contactomes throughout post-embryonic development in *C. elegans*. Connectomes
348 and contactomes are derived from volume electron microscopy (vEM) micrographs of neuropil re-
349 gions (*Witvliet et al., 2021; White et al., 1986*). These EM micrographs are information-rich and
350 have the potential to reveal architectural motifs across scales, from the nanoarchitecture of the
351 neuron to the neuroanatomy of each circuit in the brain. Cell biological features, such as con-
352 tact profiles and synaptic positions, can be rigorously quantified and systematically represented
353 as graphs capturing multidimensional relationships. These representations require methodolo-
354 gies from data science that enable dimensionality reduction and comparisons of the architecture

355 across scales. Yet to derive new intuitions about the spatiotemporal events leading to the archi-
356 tecture that shapes its function, it is necessary to integrate and compare these various representa-
357 tions, bridging knowledge from the cell biological events to the systems-level network relationships.
358 NeuroSC is designed to achieve this integration, enabling synthesis of knowledge ranging from
359 the abstractions of neuronal relationships in C-PHATE to the cell biological features underpinning
360 these abstractions. We provide a case study to illustrate how integration of analyses performed in
361 NeuroSC can result in new insights. First, we demonstrated the discovery process with C-PHATE
362 representations to identify neurons that undergo changes in their contactome during develop-
363 ment. Second, we developed 3-D representations of contact sites to analyze the local neuronal
364 regions that were identified via DC/C-PHATE analysis. Third, we visualized and compared these
365 representations across development to identify cell biological changes in neuronal morphologies
366 and synaptic positions across neuron classes. Our case study demonstrates the utility NeuroSC to
367 facilitate exploration of neuronal relationships, leading to new insights on structural features of
368 the connectome and hypotheses for empirical testing.

369 **Comparisons of NeuroSC to other connectomics atlases**

370 NeuroSC is one of several efforts centered around interpreting the *C. elegans* EM datasets. Other
371 open-source tools for data exploration in *C. elegans* include efforts to capture neuron morphologies
372 and synaptic information (including integration of new connectomes across larval development),
373 to map neurotransmitter and receptor expression, and to record whole brain functional connec-
374 tivity across genotypes (*Witvliet et al., 2021; Altun, Z.F. et al., 2002; Cook et al., 2019; Fenyves
375 et al., 2020; Randi et al., 2023; Maitin-Shepard et al., 2021; Boergens et al., 2017*). NeuroSC was
376 designed to interface and enhance these existing resources. NeuroSC focuses on comparative, bi-
377 logically grounded analysis of segmented neuronal features across datasets. This includes new
378 tools for rendering contact profiles, synchronizing 3D views, and navigating C-PHATE diagrams, all
379 of which support multi-scale comparisons of neuronal organization. NeuroSC was designed as a
380 series of modular, open-source tools that can be integrated onto other programs or existing re-
381 sources, enhancing the existing landscape of connectomic tools. NeuroSC was inspired by tools
382 like NemaNode and WormWiring (*Witvliet et al., 2021; Cook et al., 2019*), which enable 3-D visu-
383 alizations of neuronal morphologies and synaptic sites with synaptic subsets restricted to pre or
384 postsynaptic sites. In NeuroSC we sought to generate and integrate information beyond the synap-
385 tic connectome to include local neuronal regions (contactome) and neuronal morphologies across
386 available developmental vEM datasets. Contactomes represent features that have been largely
387 overlooked in connectomic datasets, and which capture circuit structures not evident by inspect-
388 ing solely synaptic relationships (*Brittin et al., 2018*). NeuroSC extends existing representations to
389 also offer user-driven experience with choice over the visualization of specific synaptic sites, the
390 option to search for synaptic partners, and the ability to customize the color of each synaptic rep-
391 resentation (Figure 7). NeuroSC representations complement resource databases like WormAtlas,
392 which hosts digitized electron micrographs and schematics of neuron morphologies with aggre-
393 gated information on each neuron (*Altun, Z.F. et al., 2002*). Neuroglancer (*Maitin-Shepard et al.,
394 2021*) developed by Google, is a powerful interactive tool for visualizing large-scale 3D electron
395 microscopy (EM) and other neuro imaging datasets beyond the *C. elegans* community. Similar in
396 functionality to Webknossos *Boergens et al. (2017)*, it provides detailed views of high-resolution
397 EM data and enables users to explore individual datasets effectively, with a strong emphasis on
398 synaptic connectivity. NeuroSC builds upon these capabilities by offering a complementary ap-
399 proach focused on comparative connectomics and broader neuronal relationships. NeuroSC en-
400 ables the visualization of EM datasets alongside neuron reconstructions while allowing users to
401 compare neuron relationships across multiple carefully curated datasets. These datasets have
402 been standardized across time points and methodologies, making it possible to track develop-
403 mental changes in neural circuits with confidence. In addition to synaptic connections, NeuroSC
404 highlights the contactome with rendered contact patches, providing a more complete picture of

405 spatial relationships. Users can dynamically adjust colors of rendered objects, generate scale bars
406 for precise comparisons, and clearly visualize synapses with large geometric representations of
407 pre- and post-synaptic structures. Importantly, neuron names and object relationships appear di-
408 rectly when hovering over a rendering, eliminating the need for external lookup tables. NeuroSC
409 also supports downloading models and creating publication-ready figures, making it a valuable
410 tool for both research and presentation. While NeuroSC does not prioritize the display of raw
411 EM data, this information is accessible through <http://NeuroSC.cytoSHOW.org/> (link also available
412 on NeuroSC.net in the "About" section) for those who want direct EM inspection. By emphasizing
413 comparability and standardized dataset integration, NeuroSC enables researchers to uncover
414 insights into neural development and connectivity that might not be as easily accessible with single-
415 dataset visualization tools. Together, existing tools and NeuroSC provide complementary ways to
416 explore and analyze complex neural datasets, each offering unique strengths to the neuroscience
417 community.

418 **NeuroSC design and future directions**

419 NeuroSC code and development was intentional in its design as an open-source resource that is
420 modular and allows integration of additional features and data structures (*Cantarelli et al., 2018*).
421 It is a hypothesis-generating tool that can be equally used by educators seeking to teach neu-
422 roanatomical principles, and researchers seeking to identify changes across connectome datasets.
423 NeuroSC could be integrated into emerging datasets, including developmental time-courses of
424 cell-specific transcriptomic data that would enable further insights on the molecular events under-
425 pinning neuronal development and function- from synaptogenic processes to the logic of neuro-
426 transmitter use (*Packer et al., 2019; Taylor et al., 2021; Fenyes et al., 2020*) and how it sustains
427 functional connectivity (*Randi et al., 2023*). Future iterations of NeuroSC could also include po-
428 sitions and relationships of neurons to non-neuronal cell types, as well as the relative networks
429 of segmented and quantified organelles within cells. NeuroSC could be used to compare new
430 datasets from genetic variants, from animals trained under specific conditions or from additional
431 developmental datasets across embryogenesis. As such, the pipeline and design of NeuroSC can
432 serve as a sandbox to examine the value of the integration of datasets in exploring representations
433 of neuronal relationships across connectomes. Currently, the addition of new datasets must be
434 performed in-house. In the future, standardized practices for EM generation and annotation data
435 could facilitate the implementation of a standard importer.

436 NeuroSC forms part of a longer tradition that has leveraged the pioneering datasets generated
437 for *C. elegans* connectomes towards exploring structure-function relationships in the nervous sys-
438 tem. While the smaller scale of the *C. elegans* neuropil allowed us to rigorously vet the utility of
439 these approaches, we suggest that these same methods would be beneficial in comparative stud-
440 ies in neuropils of other species, including those with less stereotypically formed connectomes. We
441 recognize that more complex organisms possess orders of magnitude more neurons, with signifi-
442 cantly larger neuron populations per cell class. However, our previous work has demonstrated that
443 DC/CPHATE clustering of *C. elegans* neurons consistently pulls out clusters of shared neuron classes
444 and shared functional roles (*Moyle et al. (2021)*). Building on this foundation, we envision applying
445 similar clustering approaches to larger connectomes, aiming to identify classes and functionally re-
446 lated neuronal groups in more complex nervous systems. We suggest that contact profiles, along
447 with neuron morphologies and synaptic partners, can act as 'fingerprints' for individual neurons
448 and neuron classes. These 'fingerprints' can be aligned across animals of the same species to cre-
449 ate identities for neurons. Frameworks for systematic connectomics analysis in tractable model
450 systems such as *C. elegans* are critical in laying a foundation for future analyses in other organ-
451 isms with up to a billion-fold increase in neurons (*Toga et al., 2012*). We think of these collective
452 efforts akin to the foundational work from *C. elegans* in pioneering genomic analysis and annota-
453 tions ahead of the Human Genome Project (*Stein et al., 2001; Collins and Fink, 1995*). We believe
454 that further integration of datasets in platforms like NeuroSC would be key in determining the rep-

455 resentations and features necessary for the interpretation and analyses of other connectomes.

456 **Methods and Materials**

457 **Lead Contact**

458 Further information and requests can be directed to Daniel.colon-ramos@yale.edu.

459 **Data Code and Availability**

460 Figures in this article have been generated with NeuroSC (Figures 5D, Figures 6-7, Figure S2G-I, Figure S3, Figure S4, Figure S5 A-B, Figure 8, Figures S6-S12, Videos S1-S4) and CytoSHOW (Figures 461 1-4, Figure 5A and C, Figure S1, Figure S5C). Data can be visualized via the viewer at NeuroSC.net 462 or by downloading glTF files from NeuroSC and using a glTF viewer to visualize them. Additionally, 463 the data generated for NeuroSC is available in .OBJ file format (and can be visualized from a local 464 hard drive with CytoSHOW (<http://NeuroSC.cytoshow.org/>)). All excel files for Diffusion 465 Condensation iterations and adjacency quantifications can be found in Tables S3- S13. Tutorials for NeuroSC 466 are available on NeuroSC.net upon opening the website, within the main menu of the website (Figure 467 S8), and in the supplementary materials (Figure S5-S12; Videos S1 and S3-S4). These tutorials 468 generally cover the process of engaging in analysis at and across specific developmental stages 469 by filtering the data items and adding items to viewers (Figure S10). General understanding for 470 how to use C-PHATE to analyze neuronal relationships can be found in Figure 1, Figure 4, Figure S6, 471 Video S1, and in our previous publication (*Moyle et al., 2021*). For additional information on filters 472 and in-viewer changes to the data (colors, developmental stages, downloading data) see Figure S5, 473 Figure S7, Figure S11, Figure S12, and Videos S3-S4. All code for website development is available 474 at Github (<https://github.com/colonramoslab/NeuroSCAN>) and for information on website archi- 475 tecture and data model see Figures S13-S14. 476

477 **Experimental Model and Subject Details**

478 Volume electron microscopy (vEM) data and segmentation of neurons and synapses were analyzed 479 from (*Witvliet et al., 2021; White et al., 1986; Brittin et al., 2018; Cook et al., 2019*). We analyzed 480 available EM datasets that were transversely sectioned and segmented (*Witvliet et al., 2021; Brittin 481 et al., 2021; White et al., 1986*). We deleted the CAN neurons in the L1-L3 datasets to keep these 482 datasets consistent with the legacy datasets L4 and Adult (N2U), which do not contain CAN neurons 483 (as in (*Moyle et al., 2021*)).

484 **Method Details**

485 All 3-D object isosurfaces (Morphologies (Neurons), Contacts, Synapses, C-PHATE plots) were gen- 486 erated from segmented EM datasets using a modified version of the ImageJ 3D viewer plug-in 487 (Schmid et al. 2010) implemented in CytoSHOW (<cytoshow.org>). This tool employs the marching 488 cubes algorithm for polygon-generation. All 3-D objects are first exported as wavefront (.OBJ) files 489 then converted to GL Transmission Format (.glTF) file format which does not distort the resolution 490 but compacts the file information to enable faster loading times in the web-based 3-D viewer. We 491 intentionally avoided surface smoothing to renderings to preserve the details of the raw EM data.

492 **Pixel Threshold Distance for Adjacency Profiles and Contacts**

493 We identified two challenges in compiling Electron Microscopy (EM) datasets for comparisons: 1) 494 how to uniformly capture neuronal relationships based on areas of physical adjacency (contact) 495 across datasets that have differences in volume depth and in x-y-z resolutions, and 2) how to 496 standardize across datasets in which membrane boundaries had been called using a variety of 497 methods, including contrast methods and segmentation methods (hand-drawn vs predicted via 498 centroid node expansion by a shallow convolutional neural network) (*Witvliet et al., 2021; Brittin 499 et al., 2018; White et al., 1986*). To address this, we first standardized the region of the neuropil 500 across all developmental stages as in (*Moyle et al., 2021*). Briefly, all cell bodies were deleted, and

501 we used the entry of the nerve ring neurons into the ventral cord as the posterior boundary land-
502 mark for the entire volume, focusing on the AIY Zone 2 (*Colón-Ramos et al., 2007*); slice range
503 Table S1). Previously reported adjacency profiles used 10 pixels (or 45 nm) as the pixel threshold
504 distance for the L4 (JSH) and Adult (N2U) datasets (*Moyle et al., 2021*). To account for differences in
505 resolution (x-y axis) and in calling membrane boundaries between the L4 and Adult datasets and
506 L1-L3 datasets, we designed a protocol to define the pixel threshold for each dataset. In short, for
507 two cells that are in direct contact (Figure S2 D) in the manually segmented datasets (L4 and Adult),
508 we calculated the length of overlap needed to reach from the segmented edge of one cell, across
509 the membrane, and into the adjacent cell, when the segmented area of one cell is expanded by
510 45 nm (10 pixels). This results in an average overlap of 30 nm for directly contacting cells in the
511 L4 dataset. Then, in each computationally segmented dataset (L1-L3), we empirically tested the
512 distance (e.g. 55 nm, 60 nm, 62 nm) required to achieve a similar overlap of 30 nm in direct con-
513 tact cells. That empirical number (in nm) was used for adjacency calculations and rendering of
514 contacts. The numbers were converted from nanometers into pixels to create a pixel threshold
515 distance for each dataset, and these are shown in Table S1. Once these corrections had been
516 applied, we calculated the cell-to-cell adjacency scores for all cell pairs in each dataset by using
517 the measure_adjacency algorithm from https://github.com/cabrittin/volumetric_analysis; (*Brittin
518 et al., 2018*) (Tables S8-S13). Adjacency matrices were used for Diffusion condensation (*Brugnone
519 et al., 2019*). The contact surface areas, shown in the contact stats boxes, each represent the sum
520 of the lengths of each all contact outlines for a given cell pair throughout the EM volume, multiplied
521 by the reported z axis spacing between the slices, giving units of nm².

522 **Diffusion Condensation**

523 Diffusion condensation (DC) is a dynamic, time-inhomogeneous process designed to create a se-
524 quence of multiscale data representations by condensing information over time (*Brugnone et al.,
525 2019*). The primary objective of this technique is to capture and encode meaningful abstractions
526 from high-dimensional data, facilitating tasks such as manifold learning, denoising, clustering, and
527 visualization. The underlying principle of diffusion condensation is to iteratively apply diffusion
528 operators that adapt to the evolving data representation, effectively summarizing the data at mul-
529 tiple scales. The diffusion condensation process begins with the initialization of an initial data
530 representation, typically the raw high-dimensional data or a preprocessed version. This initial rep-
531 resentation is used to construct a diffusion operator, a matrix derived from a similarity matrix that
532 reflects the local geometry of the data. The similarity metric, such as Euclidean distance or cosine
533 similarity, plays a crucial role in defining these local relationships. For contactome datasets, dis-
534 tances between neurons are determined by the pixel overlap between their segmented shapes in
535 the EM dataset. We use these distances to build a graph with weighted edges, in which the weight
536 of the edge represents the pixel overlap (the adjacency in the actual EM segmentation). Affinities
537 between neurons, which are a proxy for their distance in the graph, are then computed as now
538 revised in Box 1, Algorithm 1. This process is done iteratively as neurons cluster. Once the initial
539 diffusion operator is established, the algorithm proceeds to the diffusion step. In this step, the
540 diffusion operator is applied to the data, smoothing it by spreading information along the edges
541 of the similarity graph. This operation captures the intrinsic geometry of the data while reducing
542 noise. The specific form of the diffusion operator, such as the heat kernel or graph Laplacian, sig-
543 nificantly impacts how information is propagated during this step. Following the diffusion step,
544 the condensation step updates the data representation by aggregating diffused data points if the
545 distance between them falls below a 'merge threshold'. This step creates a more compact and ab-
546 stract representation of the data. These diffusion and condensation steps are iteratively repeated.
547 At each iteration, the diffusion operator is recomputed based on the updated diffuse data repre-
548 sentation, ensuring that the process adapts to the evolving structure of the data. The iterations
549 continue until a stopping criterion is met, such as convergence of the data representation to a
550 single point. The output of the diffusion condensation process is a sequence of multiscale data

551 representations. Each representation in this sequence captures the data at a different level of ab-
552 straction, with earlier representations preserving more detailed information and later representa-
553 tions providing more condensed summaries. This sequence of representations can be utilized for
554 various tasks, including manifold learning, denoising, clustering, and visualization. By iteratively
555 smoothing and condensing the data, diffusion condensation reveals the underlying structure of
556 high-dimensional datasets. The threshold (epsilon) used to merge data points in each iteration is
557 set as a small fraction of the spatial extent of the data: for each coordinate dimension (x, y, z), we
558 compute the range (maximum minus minimum), take the maximum of these three values, and
559 divide it by 10,000. This process is performed iteratively for each round of clustering until all data
560 points cluster into a single point. During diffusion Condensation (DC) we track the modularity of
561 the resulting clusters at each iteration and select the iteration with the highest modularity to define
562 the clusters that represent the strata *Moyle et al. (2021); Brugnone et al. (2019)*. Mathematically,
563 modularity is calculated by comparing the actual number of edges within clusters to the expected
564 number of such edges in a randomized network with the same degree distribution (Newman,2006).
565 A higher modularity value implies that nodes within the same cluster are more densely connected
566 to each other than to nodes in other clusters. A detailed algorithm description is provided in Box
567 1 and Algorithm 1.

Diffusion Condensation

Initialization:

Let $\mathbf{X} = \{x_1, x_2, \dots, x_n\}$ be the set of n data points in a high-dimensional space. Construct the affinity matrix \mathbf{A} , where A_{ij} measures the similarity between x_i and x_j . Typically,

$$A_{ij} = \exp\left(-\frac{d(x_i, x_j)^2}{2\sigma^2}\right)$$

for a chosen scale parameter σ and distance metric d . In the case of the contactome dataset, the data points represent segmented neurons, and affinities are computed using the number of shared pixels shared by pairs of neurons at their boundary.

Diffusion Operator:

Define the degree matrix \mathbf{D} as a diagonal matrix where $D_{ii} = \sum_j A_{ij}$. Construct the diffusion operator

$$\mathbf{P} = \mathbf{D}^{-1} \mathbf{A}$$

which normalizes the affinity matrix.

Diffusion Step:

Apply the diffusion operator to the data:

$$\mathbf{Y} = \mathbf{P} \mathbf{X}$$

This step smooths the data, capturing the intrinsic geometry.

Condensation Step:

After each diffusion step, merge data points that are within a small distance, ϵ , from each other to form a condensed representation. Specifically, data points y_i and y_j are merged if

$$\|y_i - y_j\| < \epsilon.$$

The threshold ϵ is computed as a small fraction of the coordinate-wise (element-wise) maximum pairwise distance among all pairs of points after the first diffusion step:

$$\epsilon = \frac{1}{10,000} \cdot \max_{i,j} \|y_i - y_j\|_\infty$$

where $\|\cdot\|_\infty$ denotes the element-wise (coordinate-wise) maximum norm.

Let $\pi : \{1, 2, \dots, n\} \rightarrow \{1, 2, \dots, k\}$ be a mapping that assigns each data point index i to a cluster index $\pi(i)$ after condensation. The condensed cluster centers are then given by

$$\mathbf{C} = \{c_1, c_2, \dots, c_k\}, \quad \text{where} \quad c_j = \frac{1}{|\pi^{-1}(j)|} \sum_{i \in \pi^{-1}(j)} y_i.$$

Modularity:

To evaluate the community structure after condensation, compute the modularity score M

$$M = \frac{1}{2m} \sum_{i,j} \left(A_{ij} - \frac{d_i d_j}{2m} \right) \delta(\pi(i), \pi(j)),$$

where:

- $d_i = \sum_j A_{ij}$ is the degree of node i ,
- $m = \frac{1}{2} \sum_{i,j} A_{ij}$ is the total edge weight in the graph, and
- $\delta(\pi(i), \pi(j)) = 1$ if $\pi(i) = \pi(j)$ (i.e., x_i and x_j belong to the same cluster), and 0 otherwise.

Iteration:

Repeat the diffusion and condensation steps, adjusting the parameter σ adaptively and keeping track of the modularity score, until all points are merged. Output iteration with highest modularity score.

Box 1: Mathematical description of Diffusion Condensation

Algorithm 1 Diffusion Condensation

- 1: **Input:** Data matrix $\mathbf{X} = \{x_1, x_2, \dots, x_n\} \in \mathbb{R}^{n \times d}$, number of iterations T , scale parameter σ , condensation threshold ϵ
- 2: **Output:** Condensed data matrix $\mathbf{X}_{\text{condensed}}$
- 3: **Initialize:** Construct affinity matrix \mathbf{A} , degree matrix \mathbf{D} , and diffusion operator \mathbf{P}
- 4: $\mathbf{A}_{ij} \leftarrow \exp\left(-\frac{d(x_i, x_j)^2}{2\sigma^2}\right)$ for all i, j
- 5: $\mathbf{D} \leftarrow \text{diag}(\sum_j \mathbf{A}_{ij})$
- 6: $\mathbf{P} \leftarrow \mathbf{D}^{-1}\mathbf{A}$
- 7: **for** iteration = 1 to T **do**
- 8: **Diffusion Step:**
 $\mathbf{Y} \leftarrow \mathbf{P}\mathbf{X}$
- 9: **Condensation Step:**
 Merge data points x_i and x_j if $d(x_i, x_j) < \epsilon$ to form
 condensed cluster centers $\mathbf{C} = \{c_1, c_2, \dots, c_k\}$
- 10: $\mathbf{X} \leftarrow \mathbf{C}$
- 11: **Update:**
- 12: $\mathbf{A}_{ij} \leftarrow \exp\left(-\frac{d(x_i, x_j)^2}{2\sigma^2}\right)$ for all i, j
- 13: $\mathbf{D} \leftarrow \text{diag}(\sum_j \mathbf{A}_{ij})$
- 14: $\mathbf{P} \leftarrow \mathbf{D}^{-1}\mathbf{A}$
- 15: **end for**
- 16: **Return:** $\mathbf{X}_{\text{condensed}} \leftarrow \mathbf{X}$

569 C-PHATE

570 C-PHATE is an extension of the PHATE technique (*Moon et al., 2019*) which is specifically aimed
571 at handling and visualizing high-dimensional biological data. C-PHATE is specifically designed to
572 handle compositional data, which are datasets where the components represent parts of a whole
573 and are inherently constrained. It learns the intrinsic manifold of the data, effectively capturing
574 non-linear relationships and structures that are not apparent with traditional methods like PCA or
575 t-SNE. The C-PHATE algorithm starts by loading affinity matrices associated with specific clustering
576 obtained from diffusion condensation. These matrices are normalized to generate kernel matrices
577 that emphasize the strength of connections within each cluster. The algorithm then builds a con-
578 nectivity matrix by integrating these kernel matrices based on cluster assignments over multiple
579 time points. This is achieved by first initializing the matrix with kernel matrices along its diagonal
580 and then filling in off-diagonal blocks with transition probabilities that reflect how clusters transi-
581 tion from one time point to the next. Next, we apply the PHATE dimensionality reduction technique
582 to the connectivity matrix to generate 3D embeddings of the data. These embeddings are derived
583 from multiple iterations of diffusion condensation, capturing the geometry of the data at various
584 levels of granularity. The resulting coordinates are saved for subsequent analysis. The final step
585 involves visualizing the PHATE results in a 3D graphics tool, CytoSHOW (Java-based; CytoSHOW.org;
586 <https://github.com/mohler/CytoSHOW>; (*Moyle et al., 2021*)). The results are plotted in a 3D envi-
587 ronment, with functionality enabling rollover labels to display information about clustered cells.
588 This requires cross-referencing output tables from the original data collection. CytoSHOW is an
589 interactive tool that allows for assigning colors and annotations to individual neurons and clusters
590 of interest. A detailed algorithm description is provided in Box 2 and Algorithm 2. The python code
591 for C-PHATE allows for user specification of four numerical parameters within the command line,
592 and we used the same set of values for all C-PHATE plots shown in this report (100, 30, 50, 1). The
593 first two integers define the weighting of connectivity between the current condensation step t

594 and previous steps t-1 (weighting = 100) or t-2 (30), respectively, during construction of the connec-
595 tivity matrix. Values 100 and 30 consistently resulted in a series of plotted clustering trajectories
596 that form a dome-like convergence of paths, enhancing our visual perception of relative rela-
597 tionships and showcasing the super clusters that constitute anatomical strata in the nerve ring neuropil
598 (Video S1). The reproducibility of the dome shape depends on assigning two specific PHATE par-
599 ameters (<https://phate.readthedocs.io/en/stable/api.html>) to non-default values when calling PHATE,
600 the “t” value is set to 50; the “randomstate” value is set to 1.

C-PHATE

Given n data points, $\mathbf{X} = \{x_1, x_2, \dots, x_n\}$, and the diffusion condensation output, consisting of $\mathbf{C}_t = \{c_1, c_2, \dots, c_k\}$ denoting the merged data points and \mathbf{A}_t denoting the affinity matrix at iteration t .

Kernel Matrix: For each iteration, t , compute the degree matrix \mathbf{D} , where $D_{ii} = \sum_j A_{ij}$. Then, normalize the affinity matrix to construct the kernel matrix \mathbf{K}_t :

$$\mathbf{K}_t = \mathbf{D}^{-1/2} \mathbf{A}_t \mathbf{D}^{-1/2}$$

Initial Connectivity Matrix: Initialize the connectivity matrix $\mathbf{C}_{\text{PHATE}}$ with zeros. Next, populate it with the kernel matrices, \mathbf{K}_t , along its diagonal, reflecting self-connections within each cluster at each time point.

Update Transition Probabilities: For each pair of adjacent time points t and $t + 1$, compute a transition probability matrix to determine how points transition between clusters C_t and C_{t+1} . Each entry p_{ij} in this matrix represents the probability of moving from cluster i at time t to cluster j at time $t + 1$. p_{ij} is calculated by counting the number of points moving from cluster i to cluster j and normalizing by the total number of points in cluster i at time t . This can be expressed as:

$$p_{ij} = \frac{\text{Number of points moving from } i \text{ to } j}{\text{Total number of points in cluster } i \text{ at time } t}$$

Use these transition probabilities to populate the off-diagonal blocks of $\mathbf{C}_{\text{PHATE}}$

Dimensionality Reduction: Apply the PHATE algorithm to the final connectivity matrix $\mathbf{C}_{\text{PHATE}}$ to obtain the low-dimensional embedding \mathbf{Y} :

$$\mathbf{Y} = \text{PHATE}(\mathbf{C}_{\text{PHATE}})$$

Visualization: Visualize low-dimensional embedding \mathbf{Y} in CytoSHOW.

601 Box 2: Mathematical description of C-PHATE

Algorithm 2 C-PHATE

- 1: **Input:** Output of the Diffusion Condensation algorithm, number of iterations T
- 2: **Output:** Low-dimensional embedding \mathbf{Y}
- 3: **Initialize:** Load affinity matrices and cluster assignments from diffusion condensation output
- 4: **for** $t = 1$ to T **do**
- 5: Load affinity matrix \mathbf{A}_t from file
- 6: Compute degree matrix \mathbf{D}_t where $D_{tii} = \sum_j A_{tij}$
- 7: Normalize to get kernel matrix $\mathbf{K}_t = \mathbf{D}_t^{-1/2} \mathbf{A}_t \mathbf{D}_t^{-1/2}$
- 8: **end for**
- 9: $\mathbf{C}_{\text{PHATE}} \leftarrow$ zero matrix with kernel matrices \mathbf{K}_t along the diagonal
- 10: **for** $t = 1$ to $T - 1$ **do**
- 11: Compute transition probabilities matrix $\mathbf{P}_{t,t+1}$ for clusters from time t to $t + 1$
- 12: $\mathbf{P}_{t,t+1}[i, j] \leftarrow \frac{\text{Number of points moving from cluster } i \text{ to cluster } j}{\text{Total number of points in cluster } i \text{ at time } t}$
- 13: Update off-diagonal blocks of $\mathbf{C}_{\text{PHATE}}$ based on $\mathbf{P}_{t,t+1}$
- 14: **end for**
- 15: Compute the PHATE embedding \mathbf{Y} from $\mathbf{C}_{\text{PHATE}}$
- 16: **Return:** \mathbf{Y}

602 **Electron Microscopy based 3-D Models**

603 To make 3-D models of neuron morphologies from vEM datasets, we created Image-J format re-
604 gions of interest (ROIs) using published segmentation data (*Witvliet et al., 2021; White et al., 1986;*
605 *Brittin et al., 2021*). For a given cell, the stack of all sectioned ROIs was then used to draw binary im-
606 age masks as input to a customized version of the marching cubes algorithm (*Schmid et al., 2010*)
607 to build and save a 3-D isosurface. All steps of this pipeline were executed within the ImageJ-based
608 Java program, CytoSHOW (*AU Duncan et al., 2019*). Slightly modified versions of this workflow were
609 also followed for: 1) generating cell-to-cell contact ROIs and 2) for generating 3-D representations
610 of synaptic objects. To align the 3-D models from the variously oriented vEM datasets, all surfaces
611 from a given specimen were rotated and resized to fit a consensus orientation and scale. This was
612 achieved by applying a rotation matrix multiplication and scaling factor to all vertex coordinates
613 in isosurfaces comprising each modeled dataset (Table S2). Each 3-D object (morphology, contact
614 or synapse) was then exported as a Wavefront file (.OBJ) and then web-optimized by conversion
615 to a Draco-compressed .GLTF file. Each neuron was assigned a type-specific color that is consis-
616 tent across all datasets to enable facile visual comparison. All the original EM annotations that
617 were used to create the representative 3D models in NeuroSC have been preserved, and can be
618 accessed via the sister app, CytoSHOW (<https://github.com/mohler/CytoSHOW>; (*AU Duncan et al.,*
619 *2019*)).

620 **Morphologies**

621 Neuron morphologies were linked across datasets for users to visualize changes over time. To en-
622 hance 3-D graphics performance without sacrificing gross morphologies we employed a defined
623 amount of data reduction when building each cell-morphology object. NeuroSC can therefore dis-
624 play multiple (or even all) neurons of a specimen within a single viewer. The number of vertices
625 for a given object was decreased by reducing 10-fold the pixel resolution of the stacked 2-D masks
626 input into the marching cubes algorithm of CytoSHOW.

627 **Nerve Ring**

628 To make a simplified mesh of the overall nerve ring shape, individual neuron ROIs were fused to-
629 gether into a single nerve-ring-scale-stack of image masks. This was used for input to the marching

630 cubes algorithm. The union of all overlapping enlarged neurite ROIs in a vEM section was data re-
631 duced (20-fold reduced pixel resolution). This rendered a performance-friendly outer shell of the
632 nerve ring.

633 Contacts

634 To build 3-D representations of neuron-neuron contacts, we captured the degree of overlap when
635 an adjacent cell outline was expanded by the specimen-specific, empirically-defined pixel threshold
636 distance listed in Table S1 (see Figure S2). This was done for each cell outline. This expansion step
637 employs a custom-written method in CytoSHOW that increases the scale of the adjacent outlined
638 region by the pixel threshold distance (Table S1; Figure S2 B and E), while maintaining its congruent
639 shape. The entire collection of captured 2-D contact overlaps (Figure S2 C and F) for each adjacent
640 neuron pair was then reconstructed as a single 3-D object (Figure S2 H). Contact patches shown in
641 NeuroSC are largely reciprocal (e.g. if there is a AIML contact from PVQL then there will be a PVQL
642 contact from AIML), but rarely, 2-D overlap regions may be too small to be reliably converted to
643 3-D isosurfaces by the marching cubes algorithm, resulting in absence of an expected reciprocal
644 contact model within the collection. Contacts, like cell morphology models, are named to be au-
645 tomatically linked across time-point datasets and to facilitate user-driven visualization of changes
646 over time.

647 Synapses

648 Synaptic positions were derived from the original datasets and segmentations, which annotate
649 synaptic sites in the EM cross-sections (*White et al., 1986; Cook et al., 2019; Witvliet et al., 2021*).
650 To represent these coordinates in the 3-D segmented neurons, we used Blocks (presynaptic sites),
651 Spheres (postsynaptic sites) and Stars (electrical synapses). The synaptic 3-D objects were placed at
652 the annotated coordinates (*White et al., 1986; Cook et al., 2019; Witvliet et al., 2021*). Additionally,
653 the objects were scaled with the scaling factor (Table S2). Synaptic objects were named by using
654 standard nomenclature across all datasets, as explained in Supplementary Figure 7.

655 We note that the L4 and Adult datasets and the L1-L3 datasets were prepared and annotated
656 by different groups (*White et al., 1986; Cook et al., 2019; Witvliet et al., 2021*). Integration of these
657 datasets reveals nanoscale disagreements in the alignment of the boundaries and synapses. Our
658 representations reflect the original annotations by the authors. Because of these disagreements
659 in annotations, the synapses are not linked across datasets. However, all the original EM annota-
660 tions that were used to create the representative 3D models in NeuroSC, including the synaptic
661 annotations, have been preserved, and can be accessed by the users via the sister app, CytoSHOW
662 (CytoSHOW.org).

663 Website Architecture

664 The NeuroSC website architecture and data structure were designed to integrate these key user-
665 driven features via a modular platform and linked datasets. The architecture uses Gepetto, an
666 open-source platform designed for neuroscience applications, modularity, and large datasets (*Cantarelli*
667 *et al., 2018*). Briefly, the architecture is effectively separated into two applications, a front end Re-
668 act/JavaScript bundle that is delivered to the client, rendering the neuron data and assets, and a
669 Golang application that exposes a JSON API, serving the neuron data and assets based on user in-
670 teractions (Supplementary Figure 13). The backend uses a Postgres Database to store underlying
671 data (Supplementary Figure 14), a Persistent Storage Volume that houses and serves static assets,
672 and a variable number of Virtual Machines to run the front end and backend application code,
673 scaling as needed to accommodate traffic. The User Interface is a React application that allows
674 users to filter, sort, and search through the Neurons so that they can be added to an interactive
675 canvas (Supplementary Figure 13). When users add Neurons to a viewer, a .gltf file is loaded in for
676 a given model (Synapses, Neurons, Contacts) at the selected developmental stage (Supplementary
677 Figure 13), which can then be manipulated in the 3D environment or layered with other meshes as

678 needed. NeuroSC can be used on common web-browsers (e.g. Google Chrome, Safari) and mobile
679 devices.

680 The underlying data model makes use of tables representing Synapses, Neurons, Contacts and
681 Developmental Stages. Relationships between these models are represented by foreign keys (Sup-
682 plementary Figure 14). Source data is defined in a file-tree structure containing various assets (such
683 as .gltf files representing various entities), as well as CSV's which store relationships across entities.
684 The directory structure outlines a vertical hierarchy, starting at the developmental stages, then
685 branching downwards onto neuron and synapse data. A Python script is invoked to traverse the
686 directory tree and parse the files, writing to the database accordingly. This configuration enables:
687 1) verification of the ingested data and 2) quick search times through the datasets to identify re-
688 lated items. Code is version-controlled in GitHub (<https://github.com/colonramoslab/NeuroSCAN>)
689 and deployed through a CI/CD pipeline when updates are committed to the main branch (Supple-
690 mentary Figure 13).

691 Acknowledgments

692 We are grateful for current and former members of the Colón-Ramos lab for their guidance and
693 suggestions, in particular, Agustín Almoril-Porras and Malcom Díaz García for assisting with data
694 formatting, Patricia Chanabá-López and Andrea Cuentas-Condori for feedback on the NeuroSC
695 website, Mayra Blakey for administrative roles in managing contracts for funding distribution, and
696 Ben Clark and Milind Singh for feedback on the paper. We also thank Stephen Larson, Dario Del
697 Piano and Zoran Sinnema (MetaCell) for initial website software development, method reporting
698 and hosting services. We thank Brandi Mattson for editing early paper drafts. We acknowledge
699 Ryan Christensen and Hari Shroff (Janelia Research Campus) and Patrick La Riviere (University of
700 Chicago) for helpful discussions and guidance for the NeuroSC website. We thank the Research
701 Center for Minority Institutions program, the Marine Biological Laboratories (MBL), and the Insti-
702 tuto de Neurobiología de la Universidad de Puerto Rico for providing meeting and brainstorming
703 platforms. D.A.C-R. acknowledges the Whitman Fellows program at MBL for providing funding and
704 space for discussions valuable to this work. Research in D.A.C-R. and W.A.M. labs was supported by
705 NIH grant R24-OD016474. This work was also funded by the NIH/NINDS grant R35 NS132156-01,
706 DP1 NS111778 and R01 NS076558-2.

707 Authorship Contributions

708 N.L.K. Conceptualization; Data curation; Investigation; Methodology; Project Administration; Vali-
709 dation; Visualization; Writing- Original Draft S.E.E. Conceptualization; Data curation; Formal Analy-
710 sis; Investigation; Project Administration; Software; Visualization; Writing- Original Draft: reviewer
711 edits; Final Draft D.B. Formal Analysis; Software; Writing - Original Draft M.W.M. Conceptualization;
712 Formal Analysis; Investigation; Project Administration; Software; Writing- Review, Editing P.A.-M.
713 Data curation; Writing- Review, Editing N.V.M. Data curation; Investigation; Writing - Review, Editing
714 S.K. Resources; Supervision J.I.E - Software development W.A.M. Conceptualization; Data curation;
715 Formal Analysis; Funding Acquisition; Methodology; Resources; Software; Validation; Writing- Re-
716 view, editing; Corresponding Author D.A.C.-R. Conceptualization; Funding Acquisition; Resources;
717 Supervision; Visualization; Writing - Review, editing; Corresponding Author

718 Competing Interests

719 Authors do not declare any competing interests.

720 Declaration of generative AI and AI-assisted technologies in the writing process.

721 During the preparation of this work the author(s) used ChatGPT in order to improve readability.
722 After using this tool, the author(s) reviewed and edited the content as needed and take full respon-
723 sibility for the content of the published article.

724 References

725 726 **Altun, Z F , Herndon, L A , Wolkow, C A , Crocker, C , Lints, R , Hall, D H (ed s), WormAtlas; 2002.** <http://www.wormatlas.org>.

727 728 729 730 731 **AU Duncan LH, AU Moyle MW, AU Shao L, AU Sengupta T, AU Ikegami R, AU Kumar A, AU Guo M, AU Christensen R, AU Santella A, AU Bao Z, AU Shroff H, AU Mohler W, AU Colón-Ramos DA.** Isotropic Light-Sheet Microscopy and Automated Cell Lineage Analyses to Catalogue *Caenorhabditis elegans* Embryogenesis with Subcellular Resolution. *JoVE*. 2019 Jun; (148):e59533. <https://www.jove.com/t/59533>, doi: 10.3791/59533, publisher: MyJoVE Corp.

732 733 734 735 **Barabási DL, Bianconi G, Bullmore E, Burgess M, Chung S, Eliassi-Rad T, George D, Kovács IA, Makse H, Nichols TE, Papadimitriou C, Sporns O, Stachenfeld K, Toroczkai Z, Towlson EK, Zador AM, Zeng H, Barabási AL, Bernard A, Buzsáki G.** Neuroscience Needs Network Science. *The Journal of Neuroscience: The Official Journal of the Society for Neuroscience*. 2023 Aug; 43(34):5989–5995. doi: 10.1523/JNEUROSCI.1014-23.2023.

736 737 738 739 **Boergens KM, Berning M, Bocklisch T, Bräunlein D, Drawitsch F, Frohnhofer J, Herold T, Otto P, Rzepka N, Werkmeister T, Werner D, Wiese G, Wissler H, Helmstaedter M.** webKnossos: efficient online 3D data annotation for connectomics. *Nature Methods*. 2017; 14(7):691–694. <https://www.nature.com/articles/nmeth.4331>, doi: 10.1038/nmeth.4331, publisher: Nature Publishing Group.

740 741 **Brittin CA, Cook SJ, Hall DH, Emmons SW, Cohen N.** A multi-scale brain map derived from whole-brain volumetric reconstructions. *Nature*. 2021 Mar; 591(7848):105–110. doi: 10.1038/s41586-021-03284-x.

742 743 **Brittin CA, Cook SJ, Hall DH, Emmons SW, Cohen N.** Volumetric reconstruction of main *Caenorhabditis elegans* neuropil at two different time points. *bioRxiv*. 2018; p. 485771. doi: 10.1101/485771.

744 745 746 **Brugnone N, Gonopolskiy A, Moyle MW, Kuchroo M, van Dijk D, Moon KR, Colon-Ramos D, Wolf G, Hirn MJ, Krishnaswamy S.** Coarse Graining of Data via Inhomogeneous Diffusion Condensation. *Proc IEEE Int Conf Big Data*. 2019 Dec; 2019:2624–2633. doi: 10.1109/BigData47090.2019.9006013.

747 748 749 **Cantarelli M, Marin B, Quintana A, Earnshaw M, Court R, Gleeson P, Dura-Bernal S, Silver RA, Idili G.** Geppetto: a reusable modular open platform for exploring neuroscience data and models. *Philosophical transactions of the Royal Society of London Series B, Biological sciences*. 2018 Sep; 373(1758). doi: 10.1098/rstb.2017.0380.

750 751 752 **Choi YK, Feng L, Jeong WK, Kim J.** Connecto-informatics at the mesoscale: current advances in image processing and analysis for mapping the brain connectivity. *Brain Informatics*. 2024 Jun; 11(1):15. <https://www.ncbi.nlm.nih.gov/pmc/articles/PMC11150223/>, doi: 10.1186/s40708-024-00228-9.

753 **Collins FS, Fink L.** The Human Genome Project. *Alcohol health and research world*. 1995; 19(3):190–195.

754 755 756 757 **Collinson LM, Bosch C, Bullen A, Burden JJ, Carzaniga R, Cheng C, Darrow MC, Fletcher G, Johnson E, Narayan K, Peddie CJ, Winn M, Wood C, Patwardhan A, Kleywegt GJ, Verkade P.** Volume EM: a quiet revolution takes shape. *Nature Methods*. 2023 Jun; 20(6):777–782. <https://www.nature.com/articles/s41592-023-01861-8>, doi: 10.1038/s41592-023-01861-8, publisher: Nature Publishing Group.

758 759 **Colón-Ramos DA, Margeta MA, Shen K.** Glia promote local synaptogenesis through UNC-6 (netrin) signaling in *C. elegans*. *Science (New York, NY)*. 2007 Oct; 318(5847):103–106. doi: 10.1126/science.1143762.

760 761 762 763 **Cook SJ, Jarrell TA, Brittin CA, Wang Y, Bloniarz AE, Yakovlev MA, Nguyen KCQ, Tang LTH, Bayer EA, Duerr JS, Bülow HE, Hobert O, Hall DH, Emmons SW.** Whole-animal connectomes of both *Caenorhabditis elegans* sexes. *Nature*. 2019 Jul; 571(7763):63–71. <https://doi.org/10.1038/s41586-019-1352-7>, doi: 10.1038/s41586-019-1352-7.

764 765 766 **Cuentas-Condori A, Mulcahy B, He S, Palumbos S, Zhen M, Miller I David M.** *C. elegans* neurons have functional dendritic spines. *eLife*. 2019 Oct; 8:e47918. <https://doi.org/10.7554/eLife.47918>, doi: 10.7554/eLife.47918, publisher: eLife Sciences Publications, Ltd.

767 768 769 770 **Dorkenwald S, Matsliah A, Sterling AR, Schlegel P, Yu Sc, McKellar CE, Lin A, Costa M, Eichler K, Yin Y, Silversmith W, Schneider-Mizell C, Jordan CS, Brittain D, Halageri A, Kuehner K, Ogedengbe O, Morey R, Gager J, Kruk K, et al.** Neuronal wiring diagram of an adult brain. *bioRxiv*. 2023 Jan; p. 2023.06.27.546656. <http://biorxiv.org/content/early/2023/07/11/2023.06.27.546656.abstract>, doi: 10.1101/2023.06.27.546656.

771 772 773 **Eberle AL, Zeidler D.** Multi-Beam Scanning Electron Microscopy for High-Throughput Imaging in Connectomics Research. *Frontiers in Neuroanatomy*. 2018 Dec; 12. <https://www.frontiersin.org/journals/neoanatomy/articles/10.3389/fnana.2018.00112/full>, doi: 10.3389/fnana.2018.00112, publisher: Frontiers.

774 **Fenyves BG**, Szilágyi GS, Vassy Z, Sóti C, Csermely P. Synaptic polarity and sign-balance prediction using gene ex-
775 pression data in the *Caenorhabditis elegans* chemical synapse neuronal connectome network. *PLOS Compu-
776 tational Biology*. 2020 Dec; 16(12):e1007974. <https://doi.org/10.1371/journal.pcbi.1007974>, doi: 10.1371/jour-
777 nal.pcbi.1007974.

778 **Flavell SW**, Raizen DM, You YJ. Behavioral States. *Genetics*. 2020; 216(2):315–332. <https://www.ncbi.nlm.nih.gov/pmc/articles/PMC7536859/>, doi: 10.1534/genetics.120.303539.

780 **Galili DS**, Jefferis GS, Costa M. Connectomics and the neural basis of behaviour. *Current opinion in insect science*. 2022 Dec; 54:100968. <https://www.ncbi.nlm.nih.gov/pmc/articles/PMC7614087/>, doi: 10.1016/j.cois.2022.100968.

783 **Hall DH**, Altun ZF, WormAtlas: The anatomy of *Caenorhabditis elegans*; 2008. Accessed May 21, 2025. <https://www.wormatlas.org>.

785 **Heinrich L**, Bennett D, Ackerman D, Park W, Bogovic J, Eckstein N, Petruccio A, Clements J, Pang S, Xu CS, Funke J, Korff W, Hess HF, Lippincott-Schwartz J, Saalfeld S, Weigel AV, COSEM Project Team. Whole-cell organelle segmentation in volume electron microscopy. *Nature*. 2021 Nov; 599(7883):141–146. doi: 10.1038/s41586-021-03977-3.

789 **Kaiser M**. Connectomes: from a sparsity of networks to large-scale databases. *Frontiers in Neuroinformatics*. 2023 Jun; 17. <https://www.frontiersin.org/journals/neuroinformatics/articles/10.3389/fninf.2023.1170337/full>, doi: 10.3389/fninf.2023.1170337, publisher: Frontiers.

792 **Kasthuri N**, Hayworth KJ, Berger DR, Schalek RL, Conchello JA, Knowles-Barley S, Lee D, Vázquez-Reina A, Kaynig V, Jones TR, Roberts M, Morgan JL, Tapia JC, Seung HS, Roncal WG, Vogelstein JT, Burns R, Sussman DL, Priebe CE, Pfister H, et al. Saturated Reconstruction of a Volume of Neocortex. *Cell*. 2015 Jul; 162(3):648–661. <https://www.sciencedirect.com/science/article/pii/S0092867415008247>, doi: 10.1016/j.cell.2015.06.054.

796 **Lichtman JW**, Pfister H, Shavit N. The big data challenges of connectomics. *Nature Neuroscience*. 2014 Nov; 17(11):1448–1454. <https://www.nature.com/articles/nn.3837>, doi: 10.1038/nn.3837, publisher: Nature Publishing Group.

799 **Maitin-Shepard J**, Baden A, Silversmith W, Perlman E, Collman F, Blakely T, Funke J, Jordan C, Falk B, Kemnitz N, tingzhao, Roat C, Castro M, Jagannathan S, moenigin, Clements J, Hoag A, Katz B, Parsons D, Wu J, et al., google/neuroglancer: Zenodo; 2021. <https://zenodo.org/records/5573294>, doi: 10.5281/zenodo.5573294.

802 **Moon KR**, van Dijk D, Wang Z, Gigante S, Burkhardt DB, Chen WS, Yim K, Elzen Avd, Hirn MJ, Coifman RR, Ivanova NB, Wolf G, Krishnaswamy S. Visualizing structure and transitions in high-dimensional biological data. *Nature Biotechnology*. 2019 Dec; 37(12):1482–1492. <https://doi.org/10.1038/s41587-019-0336-3>, doi: 10.1038/s41587-019-0336-3.

806 **Moyle MW**, Barnes KM, Kuchroo M, Gonopolskiy A, Duncan LH, Sengupta T, Shao L, Guo M, Santella A, Christensen R, Kumar A, Wu Y, Moon KR, Wolf G, Krishnaswamy S, Bao Z, Shroff H, Mohler WA, Colón-Ramos DA. Structural and developmental principles of neuropil assembly in *C. elegans*. *Nature*. 2021 Mar; 591(7848):99–104. doi: 10.1038/s41586-020-03169-5.

810 **Newman MEJ**. Modularity and community structure in networks. *Proceedings of the National Academy of Sciences of the United States of America*. 2006; 103(23):8577–8582. doi: 10.1073/pnas.0601602103.

812 **Packer JS**, Zhu Q, Huynh C, Sivaramakrishnan P, Preston E, Dueck H, Stefanik D, Tan K, Trapnell C, Kim J, Waterston RH, Murray JI. A lineage-resolved molecular atlas of *C. elegans* embryogenesis at single-cell resolution. *Science (New York, NY)*. 2019 Sep; 365(6459). doi: 10.1126/science.aax1971, place: United States.

815 **Perez AJ**, Seyedhosseini M, Deerinck TJ, Bushong EA, Panda S, Tasdizen T, Ellisman MH. A workflow for the automatic segmentation of organelles in electron microscopy image stacks. *Frontiers in Neuroanatomy*. 2014 Nov; 8. <https://www.frontiersin.org/journals/neuroanatomy/articles/10.3389/fnana.2014.00126/full>, doi: 10.3389/fnana.2014.00126, publisher: Frontiers.

819 **Phelps JS**, Hildebrand DGC, Graham BJ, Kuan AT, Thomas LA, Nguyen TM, Buhmann J, Azevedo AW, Sustar A, Agrawal S, Liu M, Shanny BL, Funke J, Tuthill JC, Lee WCA. Reconstruction of motor control circuits in adult *Drosophila* using automated transmission electron microscopy. *Cell*. 2021 Feb; 184(3):759–774.e18. [https://www.cell.com/cell/abstract/S0092-8674\(20\)31683-4](https://www.cell.com/cell/abstract/S0092-8674(20)31683-4), doi: 10.1016/j.cell.2020.12.013, publisher: Elsevier.

823 **Poole RJ**, Flames N, Cochella L. Neurogenesis in **Caenorhabditis elegans**. *Genetics*. 2024; 228(2):iyae116. <https://www.ncbi.nlm.nih.gov/pmc/articles/PMC11457946/>, doi: 10.1093/genetics/iyae116.

825 **Randi F**, Sharma AK, Dvali S, Leifer AM. Neural signal propagation atlas of *Caenorhabditis elegans*. *Nature*. 2023
826 Nov; 623(7986):406–414. <https://doi.org/10.1038/s41586-023-06683-4>. doi: 10.1038/s41586-023-06683-4.

827 **Rapti G**, Li C, Shan A, Lu Y, Shaham S. Glia initiate brain assembly through noncanonical Chimaerin-Furin axon
828 guidance in *C. elegans*. *Nature Neuroscience*. 2017 Oct; 20(10):1350–1360. doi: 10.1038/nn.4630.

829 **Rivlin PK**, Januszewski M, Longden KD, Neace E, Scheffer LK, Ordish C, Clements J, Phillips E, Smith N, Take-
830 mura S, Umayam L, Walsh C, Yakal EA, Plaza SM, Berg S, Connectomic Analysis of Mitochondria in the Cen-
831 tral Brain of *Drosophila*. *bioRxiv*; 2024. <https://www.biorxiv.org/content/10.1101/2024.04.21.590464v1>, doi:
832 10.1101/2024.04.21.590464, pages: 2024.04.21.590464 Section: New Results.

833 **Schmid B**, Schindelin J, Cardona A, Longair M, Heisenberg M. A high-level 3D visualization API for Java and Im-
834 ageJ. *BMC Bioinformatics*. 2010 May; 11(1):274. [https://doi.org/10.1186/1471-
835 2105-11-274](https://doi.org/10.1186/1471-2105-11-274). doi: 10.1186/1471-2105-11-274.

836 **Stein L**, Sternberg P, Durbin R, Thierry-Mieg J, Spieth J. WormBase: network access to the genome and biology
837 of *Caenorhabditis elegans*. *Nucleic acids research*. 2001 Jan; 29(1):82–86. doi: 10.1093/nar/29.1.82.

838 **Sulston JE**, Horvitz HR. Post-embryonic cell lineages of the nematode **Caenorhabditis elegans**. *Developmen-*
839 *tal Biology*. 1977; 56(1):110–156. doi: 10.1016/0012-1606(77)90158-0.

840 **Sulston JE**, Schierenberg E, White JG, Thomson JN. The embryonic cell lineage of the nematode *Caenorhabditis*
841 *elegans*. *Dev Biol*. 1983 Nov; 100(1):64–119. doi: 10.1016/0012-1606(83)90201-4.

842 **Sun H**, Hobert O. Temporal transitions in the postembryonic nervous system of the nematode *Caenorhab-*
843 *ditis elegans*: Recent insights and open questions. *Special Issue: Temporal patterning in the*
844 *CNS*. 2023 Jun; 142:67–80. <https://www.sciencedirect.com/science/article/pii/S1084952122001872>, doi:
845 10.1016/j.semcd.2022.05.029.

846 **Swanson LW**, Lichtman JW. From cajal to connectome and beyond. *Annual Review of Neuro-*
847 *science*. 2016; 39(Volume 39, 2016):197–216. <https://www.annualreviews.org/content/journals/10.1146/annurev-neuro-071714-033954>, doi: <https://doi.org/10.1146/annurev-neuro-071714-033954>.

849 **Taylor SR**, Santpere G, Weinreb A, Barrett A, Reilly MB, Xu C, Varol E, Oikonomou P, Glenwinkel L, McWhirter
850 R, Poff A, Basavaraju M, Rafi I, Yemini E, Cook SJ, Abrams A, Vidal B, Cros C, Tavazoie S, Sestan N,
851 et al. Molecular topography of an entire nervous system. *Cell*. 2021 Aug; 184(16):4329–4347.e23. doi:
852 10.1016/j.cell.2021.06.023.

853 **Toga AW**, Clark KA, Thompson PM, Shattuck DW, Van Horn JD. Mapping the Human Connec-
854 *tome*. *Neurosurgery*. 2012 Jul; 71(1):1–5. <https://www.ncbi.nlm.nih.gov/pmc/articles/PMC3555558/>, doi:
855 10.1227/NEU.0b013e318258e9ff.

856 **Wang C**, Vidal B, Sural S, Loer C, Aguilar GR, Merritt DM, Toker IA, Vogt MC, Cros C, Hobert O. A neurotransmitter
857 atlas of *C. elegans* males and hermaphrodites. *CSH*. 2023 Dec; <http://dx.doi.org/10.1101/2023.12.24.573258>, doi:
858 10.1101/2023.12.24.573258, publisher: Cold Spring Harbor Laboratory.

859 **White JG**, Southgate E, Thomson JN, Brenner S. The structure of the nervous system of the nematode
860 *Caenorhabditis elegans*. *Philosophical Transactions of the Royal Society of London B, Biological Sciences*.
861 1986; 314(1165):1–340. doi: doi:10.1098/rstb.1986.0056.

862 **Witvliet D**, Mulcahy B, Mitchell JK, Meirovitch Y, Berger DR, Wu Y, Liu Y, Koh WX, Parvathala R, Holmyard D,
863 Schalek RL, Shavit N, Chisholm AD, Lichtman JW, Samuel ADT, Zhen M. Connectomes across development
864 reveal principles of brain maturation. *Nature*. 2021 Aug; 596(7871):257–261. doi: 10.1038/s41586-021-03778-
865 8.

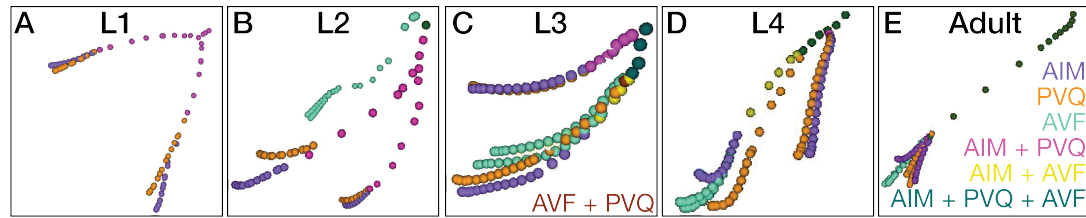
866 **Xu CS**, Hayworth KJ, Lu Z, Grob P, Hassan AM, García-Cerdán JG, Niyogi KK, Nogales E, Weinberg RJ, Hess HF.
867 Enhanced FIB-SEM systems for large-volume 3D imaging. *eLife*. 2017 May; 6:e25916. <https://doi.org/10.7554/eLife.25916>, doi: 10.7554/eLife.25916.

869 **Xu CS**, Pang S, Shtengel G, Müller A, Ritter AT, Hoffman HK, Takemura SY, Lu Z, Pasolli HA, Iyer N, Chung J,
870 Bennett D, Weigel AV, Freeman M, van Engelenburg SB, Walther TC, Farese RV, Lippincott-Schwartz J, Mellman
871 I, Solimena M, et al. An open-access volume electron microscopy atlas of whole cells and tissues. *Nature*.
872 2021 Nov; 599(7883):147–151. doi: 10.1038/s41586-021-03992-4.

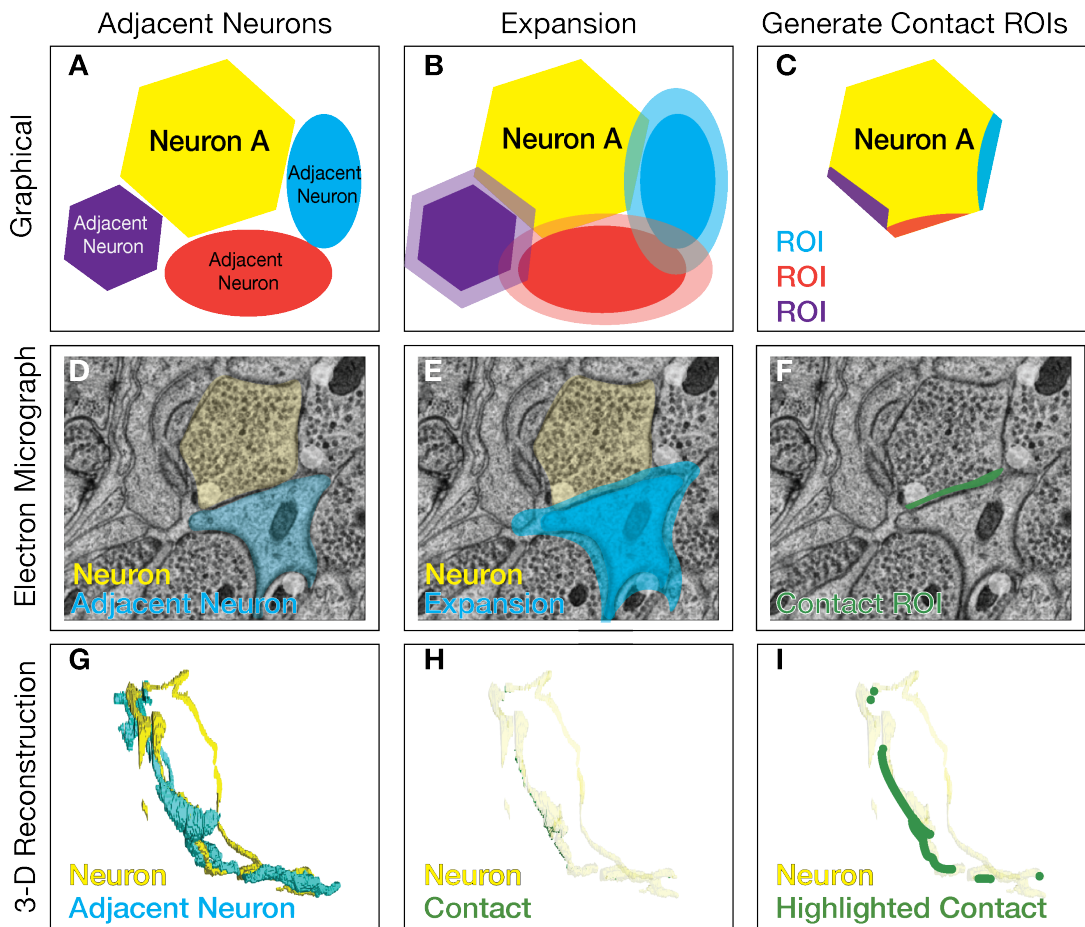
873 Zheng Z, Lauritzen JS, Perlman E, Robinson CG, Nichols M, Milkie D, Torrens O, Price J, Fisher CB, Shar-
874 ifi N, Calle-Schuler SA, Kmecova L, Ali IJ, Karsh B, Trautman ET, Bogovic JA, Hanslovsky P, Jefferis GSXE,
875 Kazhdan M, Khairy K, et al. A Complete Electron Microscopy Volume of the Brain of Adult *Drosophila*
876 *melanogaster*. *Cell*. 2018 Jul; 174(3):730–743.e22. <https://www.ncbi.nlm.nih.gov/pmc/articles/PMC6063995/>,
877 doi: 10.1016/j.cell.2018.06.019.

878 **Supplementary material**

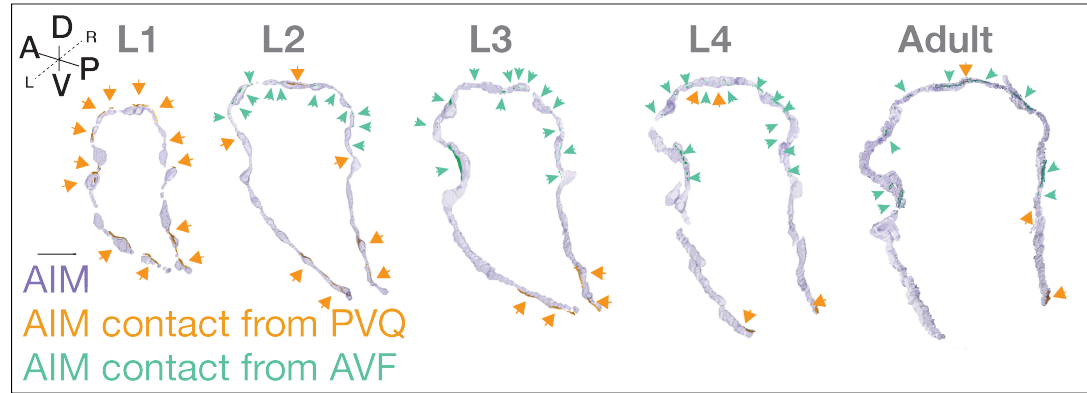
879 **Supplementary Figures**



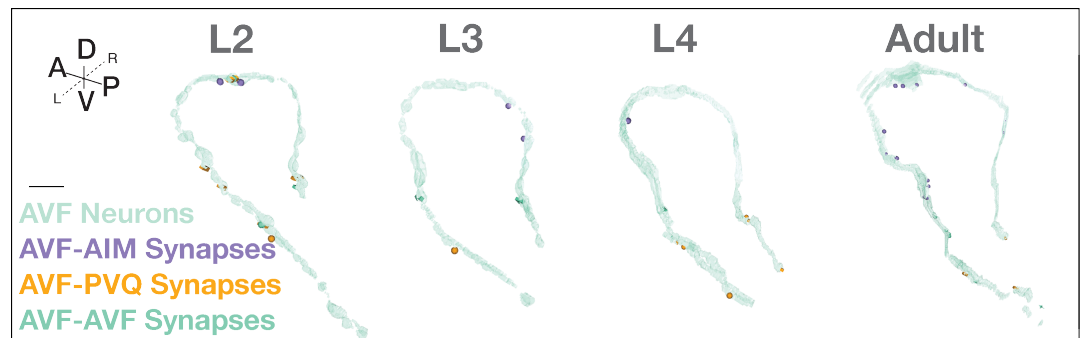
Supplementary Figure S1. DC/C-PHATE clustering of AIM, PVQ, and AVF across postembryonic development. (A-E) A cropped view of the DC/C-PHATE plot colored to identify individual neurons and clustering events in (A) Larval stage 1 (5 hours post hatching); (B) Larval stage 2 (23 hours post hatching); (C) Larval Stage 3 (27 hours post hatching); (D) Larval stage 4 (36 hours post hatching); and (E) Adult (48 hours post hatching). See also Video S1 and Table S7.



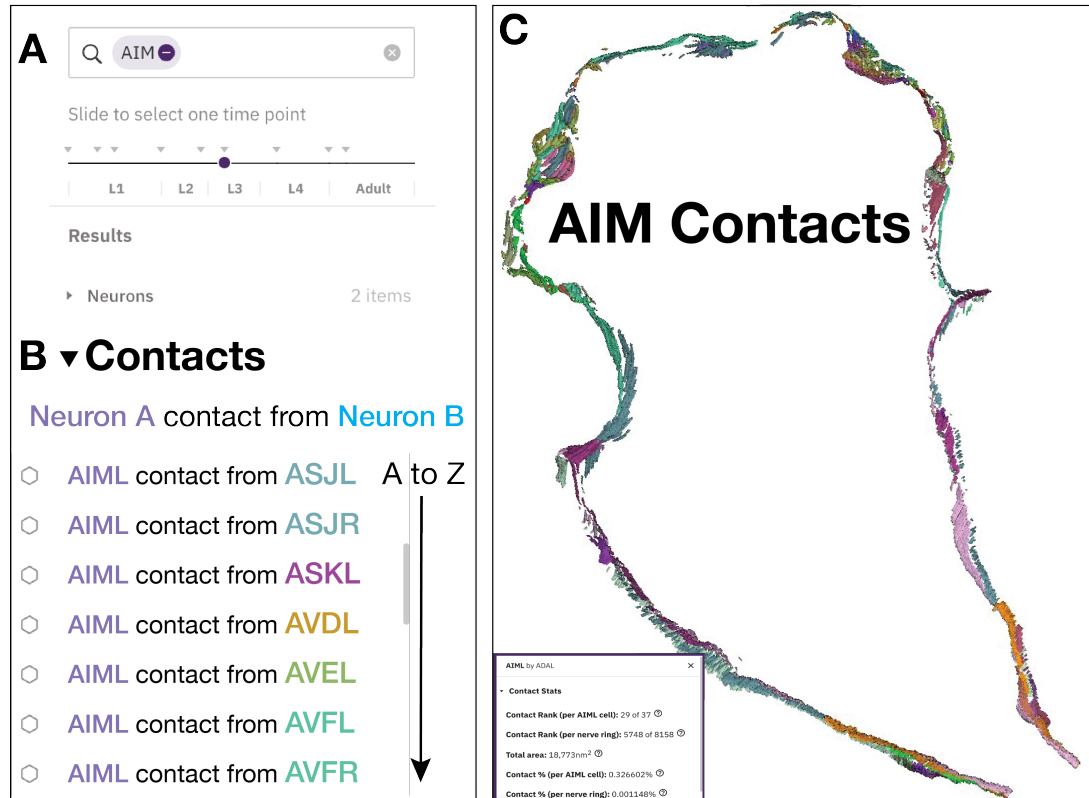
Supplementary Figure S2. Projecting contact profiles onto the segmented neuronal shapes. (A-C) Graphical representations of the strategy utilized for creating the contact profiles for each of the adjacent neurons (purple, red, cyan) onto a cross section of the neuron of interest (Neuron A, yellow). (D-F) Electron micrograph from the L4 dataset with two adjacent neurons colored yellow and cyan. To build 3-D reconstructions of contact sites from adjacent neurons, we analyzed segmented neurons from the electron microscopy datasets in each slice (A, D). Each adjacent neuron is expanded in all directions to the pixel threshold distance (specified for each dataset; Table S1; Methods; CytoSHOW.org) (B, E). A new ROI (region of interest; purple, red, cyan in C; green in F) is created from the overlapping areas between the neuron of interest (yellow) and the adjacent neurons (C,F). (G-I) 3-D reconstruction of neuron (yellow) (G) with adjacent neuron (cyan), (H) with contact sites captured (green) across all slices, and (I) with contact areas from the adjacent neuron augmented (green) as seen in Figure 5 D.



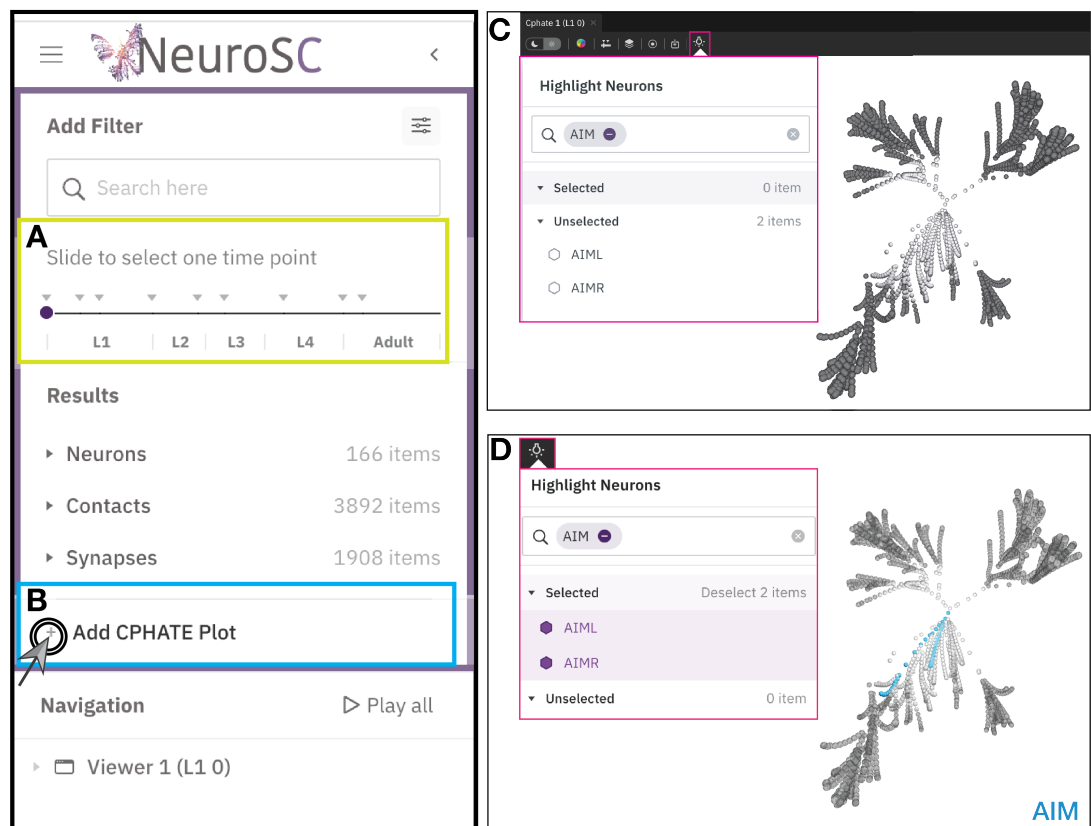
Supplementary Figure S3. AIM contact sites. Contact sites from PVQ (Orange and highlighted with orange arrowheads) and from AVF (Green and highlighted with green arrowheads) across developmental stages (as indicated) and projected onto the segmented AIM neurons (transparent purple). This figure is the unmodified NeuroSC outputs of contact profiles that corresponds to Figure 5D. In Figure 5D these contact profiles were augmented. Scale bar = 2 um. See also Figure 5 and Video S4.



Supplementary Figure S4. AVF synaptic sites. Synaptic sites displayed onto transparent (green) AVF neurons across developmental stages. Presynaptic sites (spheres) and postsynaptic sites (Blocks) are visualized between the AVF neurons and the AIM (Purple) neurons, PVQ (Orange) neurons and other AVF (either AVFL or AVFR; opaque green) neuron; Scale bar = 2 um.



Supplementary Figure S5. Visualization of contact sites in NeuroSC. (A) Search for a specific neuron (here, AIM) to filter (B) the list of contacts corresponding to the developmental slider. Neuron A (AIML, here) is the neuron onto which the contacts will be mapped. The Contacts drop down menu sorts neurons alphabetically (here, colored according to the contact patch color in C). (C) 3-D reconstruction of all AIM contacts at L3 stage. See also Video S3-S4. In the Figure 5D, contacts are augmented. Inset: Click on a contact rendering to show 'contact stats'. This pop up displays quantifications of the selected contact relationship. Rank compares the summed surface area of contacts ("patches") between these two neurons relative to all other contact relationships for the primary neuron. A rank of 1 means this neuron pair shares the largest contact area. Total surface area is the total surface area in nm² that covers the primary neuron in the contact relationship. Here the primary neuron is AIM. Contact area percentages are also shown for the cell and the whole nerve ring.



Supplementary Figure S6. C-PHATE tutorial in NeuroSC. (A) Add the C-PHATE plot corresponding to the position of the purple circle on the developmental slider (yellow box) by clicking (B) the + sign. (C) Screenshot of C-PHATE plot at L4 (36 hours post hatching), spheres represent individual neurons at the outer edge of the plot and DC iterations increase towards the center where spheres represent clusters of neurons and eventually the entire nerve ring. (D) Screenshot of C-PHATE plot at L4 (36 hours post hatching) with the spheres/clusters containing the AIM neurons highlighted (Blue) by selecting the AIM neurons within the light bulb menu (red box). See also Video S1. NeuroSC features in this figure are not shown to scale.

Supplementary Figure S7. Visualization of synaptic sites with NeuroSC. (A) Search for synaptic sites for specific neuron(s) (e.g., AIM, PVQ) and choose a developmental time point with the slider. (B) Synapses dropdown menu contains a list of objects representing pre- and postsynaptic sites corresponding to all neuron names in the search bar and sorted alphabetically. Searched neurons can be used with the synaptic filter (C) to select for synapse type (electrical or chemical; Note: only use this feature for L4_36 hours post hatching and Adult_48 hours post hatching) and to filter objects by synaptic specialization (pre or post; gray dotted box), (D) which will follow the filter logic (example shown for AIM and PVQ). (E) To enable visualization of subsets of synapses and differentiate between pre- and postsynaptic sites, each synapse contains object(s) representing the postsynaptic site(s) as spheres (Blue and Purple) and the presynaptic site as a block (Orange). These are ordered “by synapse”, with all postsynaptic objects, then the presynaptic object. This specific example corresponds to a 3-D representation of the PVQL (Orange, Pre) AIML (Blue, Post), AIML (Purple, Post) synapse. (F) All synaptic sites contain the name of the presynaptic neuron (Orange), neuron type (chemical, electrical, or undefined), list of postsynaptic neuron(s) (Blue), and Unique identifier (Black; Section, letter) for cases with multiple synapses between the same neurons. The ‘section’ is unique to each synapse between specified neurons and at that specific developmental stage. It is listed in order of its antero-posterior position in the neuron. Synapse names are not linked through developmental datasets. If the synapse is polyadic, there will be multiple postsynaptic neuron names and objects associated with a single presynaptic site. See also Video S4. (G) Right click on a rendered synapse to open synapse stats. Expand (click arrow in green box) to show the numbers of synapses, broken down by polyadic variations if applicable, per the primary neuron (in this case the primary neuron is PVQL).

A

Opening Page

NeuroSC

Add Filter

Search here

Slide to select one time point

L1 L2 L3 L4 Adult

Results

- ▶ Neurons 197 items
- ▶ Contacts 8158 items
- ▶ Synapses 1829 items
- ▶ Nerve Ring (add last) 1 items

+ Add CPHATE Plot

Navigation

Play all

No viewers added yet

Nothing to display yet.
You can search for neurons, contacts and synapses using the left sidebar.

B Menu

NeuroSC

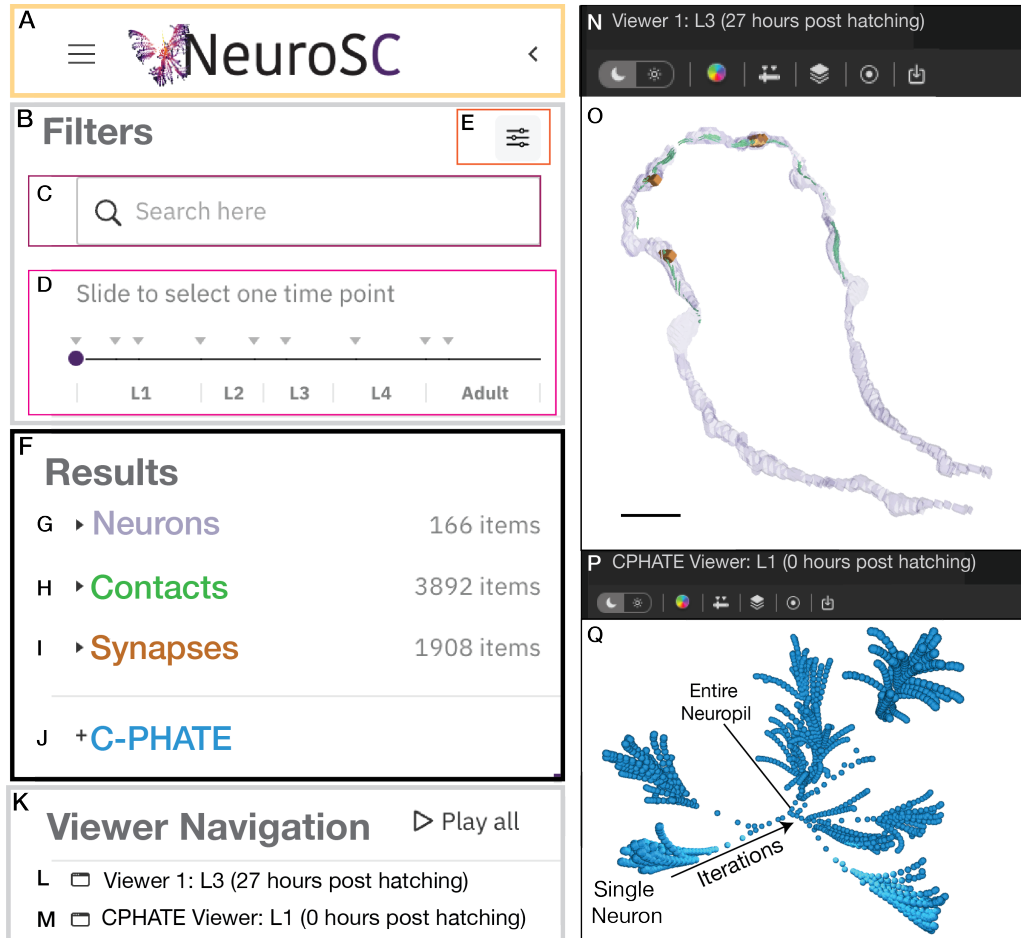
About NeuroSC

Tutorial

Promoter DB

Nothing to display yet.
You can search for neurons, contacts and synapses using the left sidebar.

Supplementary Figure S8. Opening page view and menu.(A) View of opening page. (B) Menu for access to the 'About' window for referencing source information, the Tutorial, and the developmental Promoter database. See also Video S3.



Supplementary Figure S9. The NeuroSC interface enables interrogation of neuronal relationships across development. (A) The left facing arrow to minimize the left panel and optimize space for the viewer windows. The interface contains four main parts: (B-E) Filters, (F-J) Results, (K-M) Viewer Navigation, and (N-Q) viewer windows. Filter Results by (C) searching for neuron names, (D) selecting a dataset with the developmental slider (in hours post- hatching), (E) and filtering synapses based on the pre- or post-synaptic partner on the neurons that are on the search bar. (F) Results drop down menus (filtered by B) for (G) Neuronal morphologies (shown in the viewer as purple in (O)), (H) Contacts (shown in green (O)); (I) Synapses (shown in Orange in (O)); and (J) C-PHATE (shown in (Q)), which gets filtered by the developmental slider in (D). (K) Viewer Navigation to rotate the 3-D projections in all viewers simultaneously (Play All) and which contains a drop-down menu for each viewer (L,M). The viewers are named as Viewer 1 (L, N) or CPHATE viewer (M, P) and followed by information of the developmental stage and the hours post hatching for the objects in the viewer. (O) Reconstruction of the AIM neurons with AVF contacts and synapses at L3 (27 hours post hatching; scale bar = 2 um. (Q) C-PHATE plot at L1 (0 hours post hatching). See also Video S3.

Select and Add Items to Viewer

Select

Add item(s) to a viewer

Select viewer

All Items

Individual Items

OR

OR

Deselect items

A

B

C

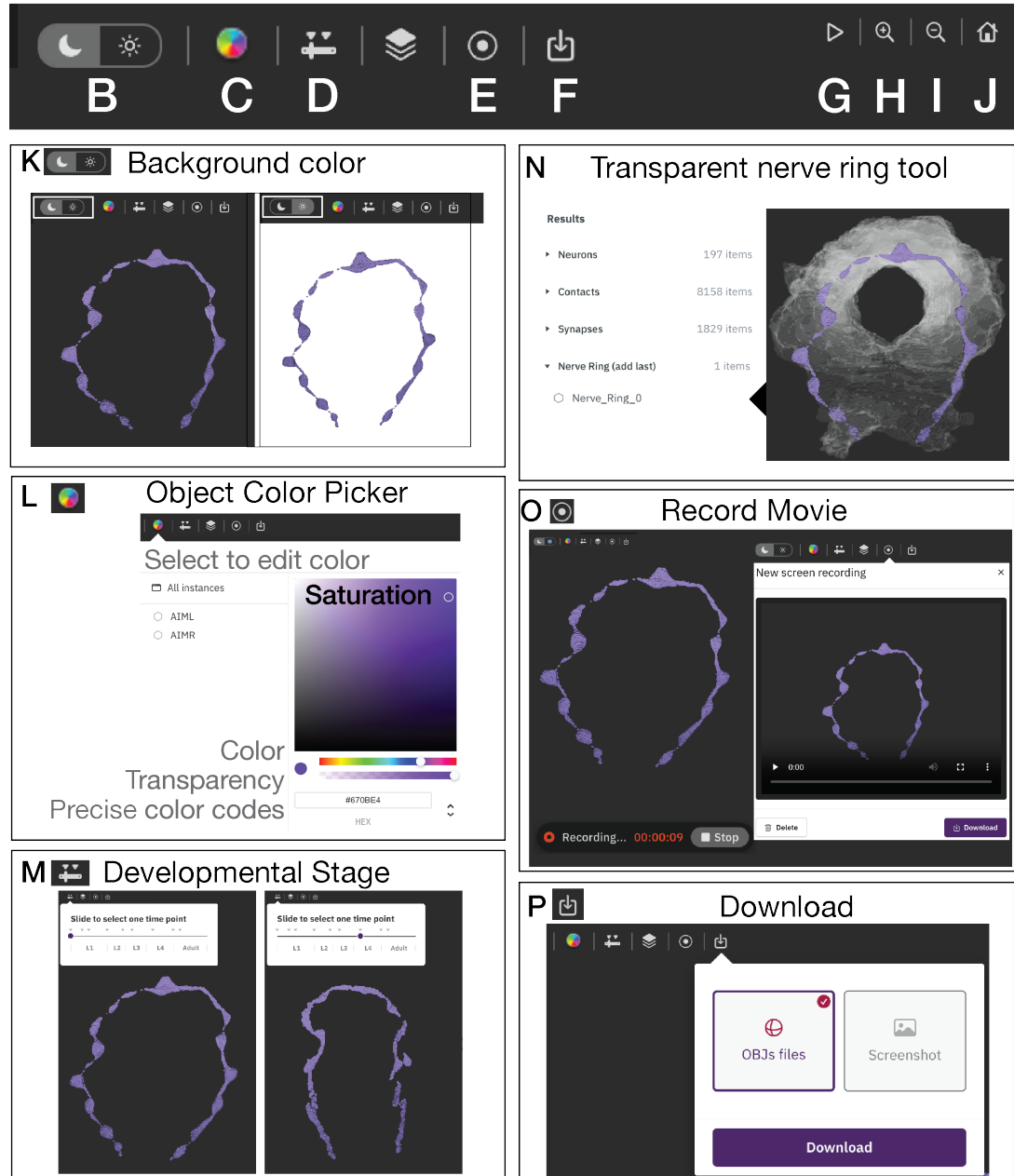
A'

B'

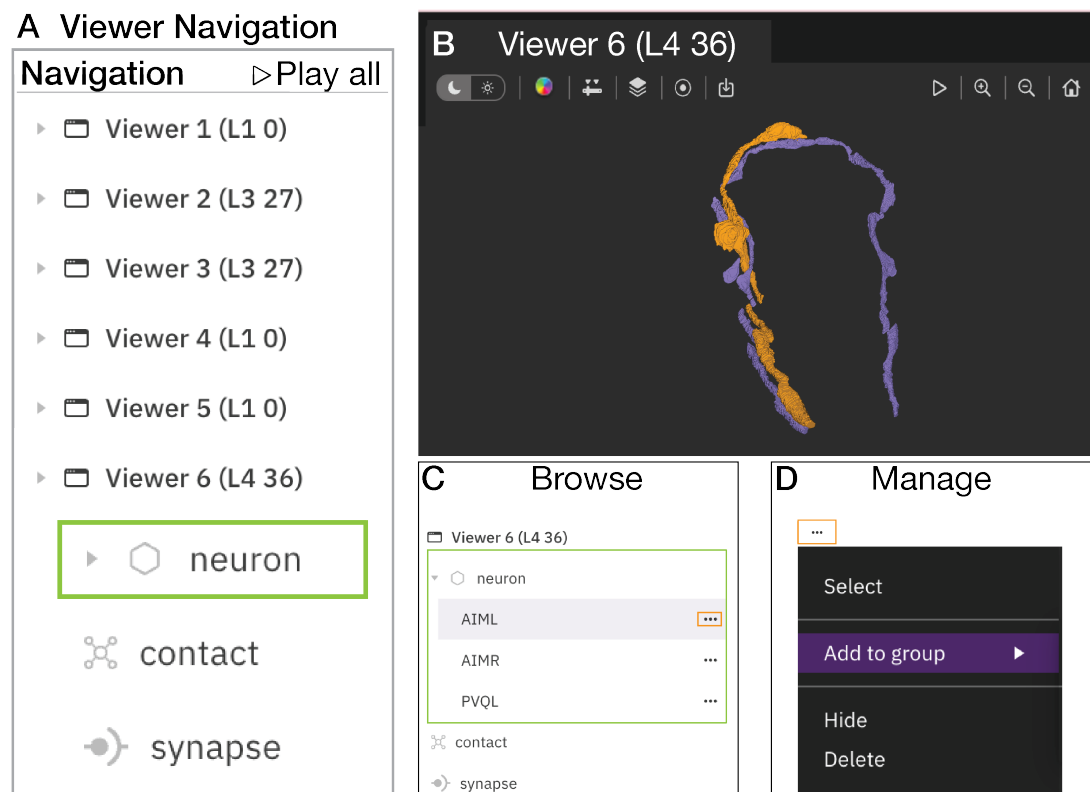
D

Supplementary Figure S10. Select and Add objects to viewers. (A) Click “select (number) items” to select all items in the drop down list (green box), or (A') click the hexagon next to each item (green box). (B) Click “Add Selected” (purple box) to add all selected items or (B') click “Add to” (purple box) to add each item individually. (C) To add the selected item(s) to an existing viewer of the same developmental stage or to a new viewer, choose a viewer as indicated. (D) Click “Deselect (number) items” (orange box) to deselect items. See also Video S3 and S4.

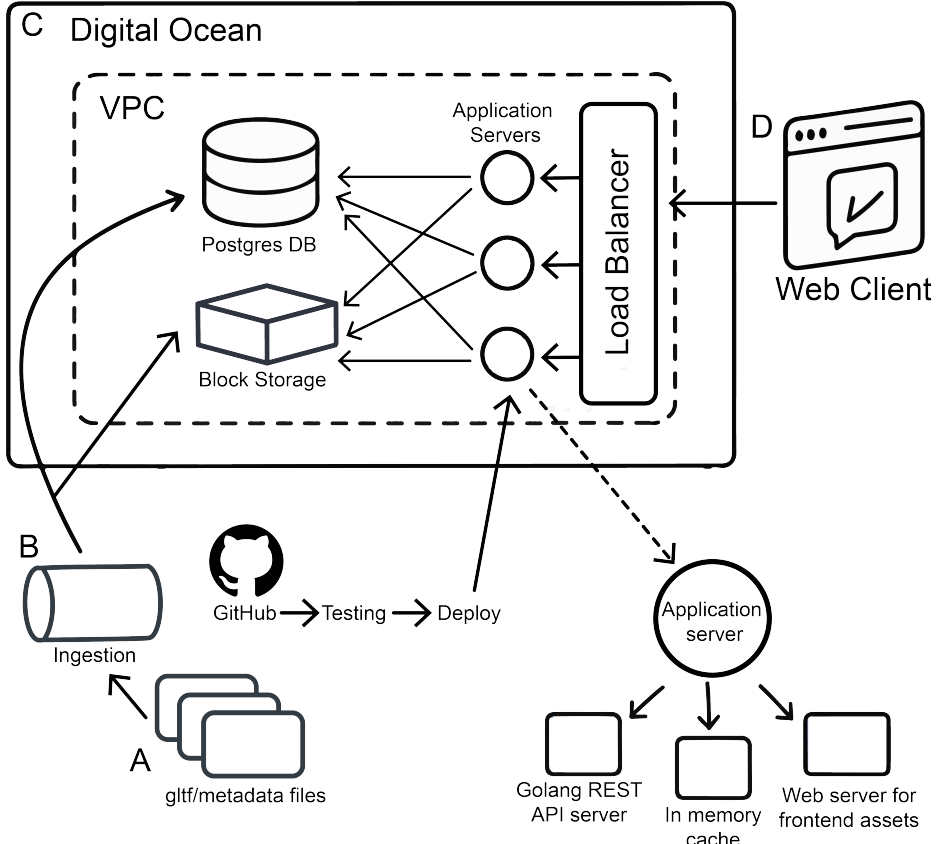
A In-Viewer Toolbar



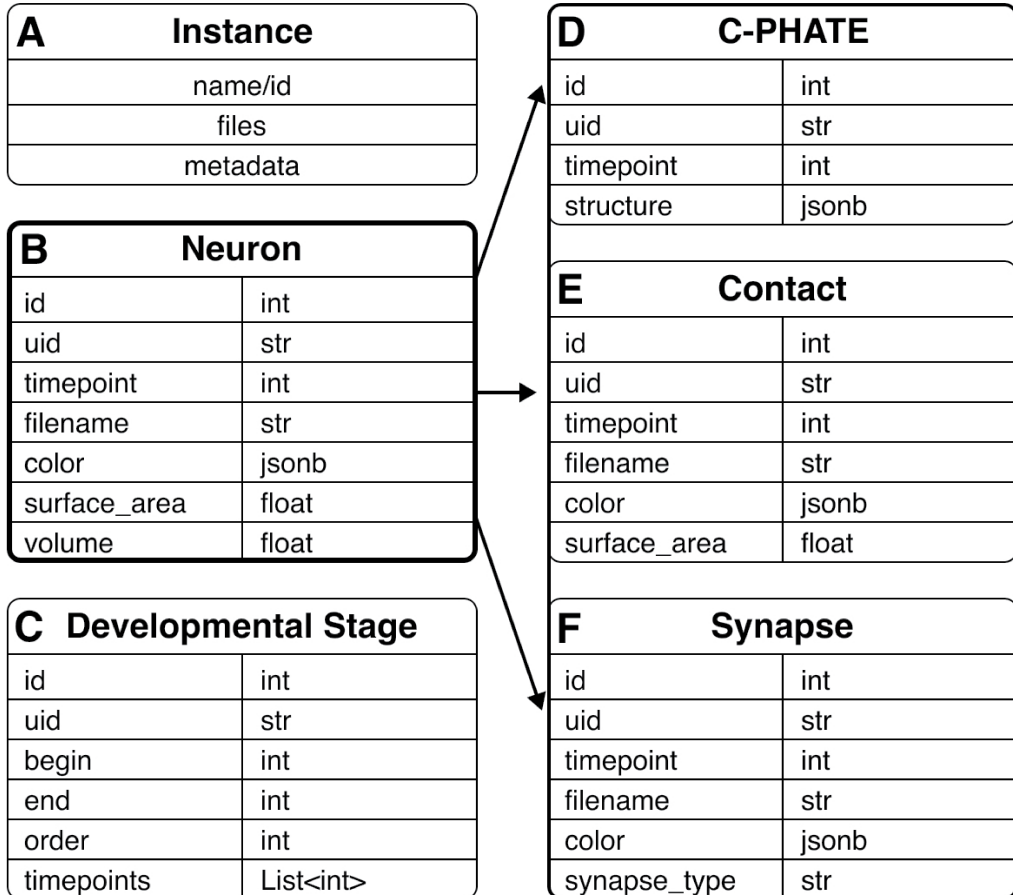
Supplementary Figure S11. In-viewer toolbar features (A) In-viewer toolbar for Neurons, Contacts and Synapses and C-PHATE (shown here, only Neurons). (B, K) Change the background color of viewer from dark (white box, moon) to white (white box, sun). (C, L) Change the color of any objects by selecting a desired color, transparency or color code and selecting the object (or instance) name (here, AIML and AIMR). (D, M) Copy and paste your neuron and contact profile scenes through time into a comparative side by side window changing the developmental stage for items in the viewer by using the in-viewer developmental slider. Note a new window will be generated, which can be dragged next to the original window. (N) Add 3-D representations of the Nerve Ring for that developmental stage, note: must be added to the scene last. (E, O) Record and download movies for the viewer. (F, P) Download .gltf files and viewer screenshot (png). (G) Rotate objects around the y-axis. (H) Zoom in and (I) zoom out, and (J) reset objects to original positions in the viewer. See also Video S3.



Supplementary Figure S12. Viewer navigation menu. ((A) Navigation bar contains a drop-down menu for each viewer (shown here, six viewers at varied developmental stages) and a “Play all” button for simultaneously rotating all objects in each viewer around the y-axis (Video S3). Each viewer drop down menu contains a drop down menu for Neurons (green box), Contacts and Synapses. (B) Viewer 6 with reconstructions of three neurons (AIML and AIMR, purple; PVQL, orange) at Larval Stage 4 (L4), 36 hours post hatching. (C) Browse and Select objects in the viewer by navigating the nested drop down menus. (D) Manage objects in viewers with options to select, group, hide, and delete objects in each viewer. Objects can be deleted with “select” and keyboard “delete”. See also Video S3.



Supplementary Figure S13. NeuroSC architecture. (A) Source data are defined in a file tree structure that contains various assets such as .gltf files representing various entities, as well as CSVs storing entity metadata. The directory structure outlines a vertical hierarchy starting at the developmental stages, then branching downwards through neuron, C-PHATE, contact and synapse data.(B) A Golang script can be invoked to traverse the directory tree and ingest the files. This parses the hierarchical file path and file contents, verifying the data and associating it with underlying entities, writing it to the database.(C) The backend consists of a Postgres Database to store underlying data, a Block Storage Volume that houses static assets (.gltf files, javascript bundle, css styles, etc), and a Golang application. The Golang application surfaces a JSON REST API, leveraging caching strategies to reduce DB load. It also serves the static assets to the client, from the block storage. A variable number of Virtual Machines run the backend application code, scaling as needed to accommodate traffic.(D) The client-side is a React application that uses Geppetto for entity rendering (Cantarelli et al. 2018). User interactions on the frontend result in queries to the backend to filter, sort, and search via the REST API, resulting in the entities and metadata to be rendered to an interactive canvas.



Supplementary Figure S14. NeuroSC data model. (A) Reference scheme for B-F; Instance refers to the category (e.g., B, Neuron; C, Developmental Stage), which contains a name or identifier (id) for each object, lists of files associated with the instance (C, Developmental Stage does not have files), and metadata to further describe each instance, which is usually a string (str) or an integer (int). (B) The neuron name is the foundation for the Contacts, Synapses, and C-PHATE, which enables integration across each of these representations and across developmental stages (time points) with metadata from WormAtlas (wormatlas.org/MoW_builtin0.92/MoW.html). (C) The Developmental Stages are named by the larval stages (L1, L2, L3, L4, Adult), and the metadata captures the list of time points within those developmental stages (i.e., L1, 0 hours post hatching, and L1, 5 hours post hatching). (D) C-PHATE objects are named with a list of Neurons. (E) Contacts link to the Neuron names (Neuron A and Neuron B nomenclature in Figure S5), and metadata annotates the surface area in nm² of contact quantified in the source Electron Microscopy micrographs. (F) Synapses link to the Neuron names (Pre, type (chemical, elecrica or undefined), Post, and section described in Figure S7).

880 **Supplementary Videos**

881 **Video S1. Visualization of hierarchical relationships using C-PHATE plots in NeuroSC.** The
882 process for rendering a C-PHATE plot at the L4 stage (36 hours post hatching) with the real-time
883 loading speed. In the viewer, 3-D visualization of a C-PHATE plot (shades of cyan), which is ro-
884 tated to show the dome-shape of the plots and to orient the plot to correspond to Figures 2 and
885 4. The highlight functionality is used to show the spheres containing AIM (teal), then PVQ (teal).
886 The spheres of the first iterations, containing AIM and PVQ, are identified, selected and colored
887 magenta. The AVF neurons are highlighted in teal, and the first AIM and AVF containing clusters
888 are identified, selected and colored yellow. The first clusters containing AIML, AVF and PVQL are
889 identified and colored green. Neurons in the left yellow and magenta clusters are reconstructed
890 with a right click on the sphere and “Add to new viewer” selection.

891 **Video S2. Analysis of AIM, PVQ and AVF neuronal morphologies in developmental datasets.**
892 3-D visualizations of AIM (Purple), PVQ (Orange) and AVF (Green) at (Left viewer) L1 (5 hours post
893 hatching) and (Right viewer) L3 (27 hours post hatching) in NeuroSC. Note that at L1, AVF has not
894 grown into the nerve ring, therefore, only AIM and PVQ are present, but by L3, the AVF neurons
895 have grown between the AIM and PVQ neurons.

896 **Video S3. Navigating NeuroSC features that enable integration of Neurons, Contacts and**
897 **Synapses across developmental datasets.** Upon first opening NeuroSC, a tutorial will launch
898 (Figure S8). In the NeuroSC menu one can read about NeuroSC, access the tutorial, and navigate
899 to the embryonic promoter database (Figure S8). The video shows the user searching neurons (AIM
900 and PVQ) and adding neurons to the viewers (Figure S10). Side-by-side viewers with AIML, AIMR,
901 and PVQL enable comparisons across developmental stages (L1, 0 hours post hatching and L4, 36
902 hours post hatching). Also shown in the video are the use of the in-viewer toolbar (Figure S11) and
903 navigation menu (Figure S12) for object exploration.

904 **Video S4. Exploring Contacts and Synapses using NeuroSCAN.** Video of user navigating the
905 tools of NeuroSC to examine synapses and contact profiles to yield results as in (Figures S7 and S9).
906 AIM neurons (Transparent Purple), AIM (Purple)-PVQ synaptic sites (Orange), and AIM-PVQ contact
907 sites (Orange) at L1 (5 hours post hatching) are added into Viewer 1. AIM neurons (Transparent
908 Purple), AIM(Purple)-PVQ synaptic sites (Orange), and AIM-PVQ contact sites (Orange), AVF (Green)-
909 AIM synaptic sites, and AVF-AIM contact sites (Green) at L3 (27 hours post hatching) are added into
910 Viewer 2. Contact sites and synaptic sites are compared across developmental stages by hiding
911 AIM neurons. All contact sites for AIM are added for L1 (5 hours post hatching) into Viewer 3.

912 **Supplementary Tables**

913 **Table S1.** Nerve ring regions, resolutions, and pixel threshold distances used to calculate adjacency
914 matrices and to create contact sites for each dataset.

915 **Table S2.** Scaling factors and rotation corrections for 3-D representations of Neurons, Contacts
916 and Synapses for each dataset.

917 **Table S3.** Stratum 1 (Red) Sankey diagrams of clustered neurons for each Diffusion Condensa-
918 tion iteration in each dataset.

919 **Table S4.** Stratum 2 (Purple) Sankey diagrams of clustered neurons for each Diffusion Conden-
920 sation iteration in each dataset.

921 **Table S5.** Stratum 3 (Blue) Sankey diagrams of clustered neurons for each Diffusion Condensa-
922 tion iteration in each dataset.

923 **Table S6.** Stratum 4 (Green) Sankey diagrams of clustered neurons for each Diffusion Conden-
924 sation iteration in each dataset.

925 **Table S7.** Sankey diagrams of AIM, PVQ and AVF containing clusters for each Diffusion Conden-
926 sation iteration in each dataset.

927 **Tables S8.** L1 (0 hours post hatching) adjacency counts and searchable counter for summed
928 adjacencies. Type the name of a “Neuron of Interest” (NOI) in the indicated cell to filter for the
929 summed adjacency counts for each contact partner. For each partner, there are two columns:

930 Total number of contacts (number of EM sections NOI and partner are in contact) and Total Weights
931 (summed number of pixels NOI and partner contacts).

932 **Tables S9.** L1 (5 hours post hatching) adjacency counts and searchable counter for summed
933 adjacencies. Type the name of a “Neuron of Interest” (NOI) in the indicated cell to filter for the
934 summed adjacency counts for each contact partner. For each partner, there are two columns:
935 Total number of contacts (number of EM sections NOI and partner are in contact) and Total Weights
936 (summed number of pixels NOI and partner contacts).

937 **Tables S10.** L2 (23 hours post hatching) adjacency counts and searchable counter for summed
938 adjacencies. Type the name of a “Neuron of Interest” (NOI) in the indicated cell to filter for the
939 summed adjacency counts for each contact partner. For each partner, there are two columns:
940 Total number of contacts (number of EM sections NOI and partner are in contact) and Total Weights
941 (summed number of pixels NOI and partner contacts).

942 **Tables S11.** L3 (27 hours post hatching) adjacency counts and searchable counter for summed
943 adjacencies. Type the name of a “Neuron of Interest” (NOI) in the indicated cell to filter for the
944 summed adjacency counts for each contact partner. For each partner, there are two columns:
945 Total number of contacts (number of EM sections NOI and partner are in contact) and Total Weights
946 (summed number of pixels NOI and partner contacts).

947 **Tables S12.** L4 (36 hours post hatching) adjacency counts and searchable counter for summed
948 adjacencies. Type the name of a “Neuron of Interest” (NOI) in the indicated cell to filter for the
949 summed adjacency counts for each contact partner. For each partner, there are two columns:
950 Total number of contacts (number of EM sections NOI and partner are in contact) and Total Weights
951 (summed number of pixels NOI and partner contacts).

952 **Tables S13.** Adult (48 hours post hatching) adjacency counts and searchable counter for summed
953 adjacencies. Type the name of a “Neuron of Interest” (NOI) in the indicated cell to filter for the
954 summed adjacency counts for each contact partner. For each partner, there are two columns: To-
955 tal number of contacts (number of EM sections NOI and partner are in contact) and Total Weights
956 (summed number of pixels NOI and partner contacts).